Precambrian Research 384 (2023) 106944

Contents lists available at ScienceDirect

Precambrian Research

journal homepage: www.elsevier.com/locate/precamres

# Geochronological constraints for a two-stage history of the Sveconorwegian rare-element pegmatite province formation

N. Rosing-Schow [a], R.L. Romer [b], A. Müller [a,c,*], F. Corfu [d], R. Škoda [e], H. Friis [a]

[a] Natural History Museum, University of Oslo, P.O. Box 1172 Blindern, 0318 Oslo, Norway
[b] GFZ German Research Centre for Geosciences, Telegrafenberg, 14473 Potsdam, Germany
[c] Natural History Museum, Cromwell Road, London SW7 5BD, United Kingdom
[d] University of Oslo, P.O. Box 1047 Blindern, 0316 Oslo, Norway
[e] University of Masaryk, Kotlářská 267/2, 611 37 Brno, Czech Republic

ARTICLE INFO

*Keywords:*
Pegmatite
U-Pb dating
Columbite group minerals
Monazite
Sveconorwegian orogen
Grenville orogen

ABSTRACT

Most pegmatites of southern Norway seem to be derived from anatectic melting of metamorphic rocks during the Sveconorwegian orogeny rather than to be highly evolved residual melts derived from granites. We test this hypothesis by providing new age data for thirteen pegmatites and one granite. Based on these new age data, we distinguish two age groups of Sveconorwegian pegmatites (>1,000 $m^3$ in size); Group 1: 1100–1030 Ma and Group 2: 930–890 Ma. All pegmatites except those from the Østfold area crystallized significantly earlier or later than adjacent granites. The Tørdal granite, yielding an age of 946 ± 4 Ma, is about 40 Ma older than the adjacent pegmatites. Field evidence and the age difference between pegmatites and granites supports an anatectic origin for these pegmatites. Sources of these pegmatite melts are biotite- and biotite-amphibole gneisses and amphibolites. Group 1 pegmatites formed in transpressional regimes after peak metamorphism, whereas Group 2 pegmatites formed in an extensional regime and the required heat for partial melting was provided by mafic magma underplating.

Differences in the rheological behavior of amphibolite and granitic gneiss during extensional tectonics are the major reason why Group 2 pegmatites occur preferentially in large amphibolite bodies. Under mid-crustal conditions, amphibolite reacts brittle to semi-brittle forming open structures in an extensional tectonic regime where partial melts drained into. Granitic gneisses react in a ductile manner and do not have the ability to drain partial melt.

Pegmatite formation in the Grenville Province, i.e., the Laurentian part of the Grenville–Sveconorwegian orogenic belt, formed between ca. 1090 and 980 Ma peaking at 1010 to 980 Ma. Thus, the Grenville peak postdates the Sveconorwegian Group 1 peak by about 30 Ma. These pegmatites formed in similar orogenic settings, implying that similar tectono-metamorphic developments along the Grenville–Sveconorwegian orogenic belt were diachronous.

We conclude that local anatexis is the major pegmatite-melt forming process in the Sveconorwegian as well as Grenville orogen. Local anatexis also may be important in other pegmatite provinces.

## 1. Introduction

Swarms of pegmatites, which commonly occur in and around granitic intrusions (Černý, 1991a; Černý and Ercit, 2005), are expressions of orogenic processes in collisional settings. In contrast to large-volume granite magmatism, the importance of these small-volume melt forming events within orogenic cycles is commonly underestimated. This is caused by two main factors. First, accurate and precise dating of pegmatites is still challenging as most minerals commonly used for U–Pb dating are often extremely rich in U, and thus metamict. Recent improvements of geochronological methods, such as the introduction of chemical abrasion (CA) TIMS (e.g., Mattinson, 2011), *in situ* Rb-Sr dating by LA-ICP-MS/MS (e.g., Karlsson and Zack, 2017) and the use of a variety of less common minerals for dating help to overcome these challenges. Second, the prevalent model of pegmatite genesis, which states that pegmatites form from the residual, most fractionated melt of large-

* Corresponding author at: Natural History Museum, University of Oslo, P.O. Box 1172 Blindern, 0318 Oslo, Norway.
*E-mail address:* a.b.muller@nhm.uio.no (A. Müller).

https://doi.org/10.1016/j.precamres.2022.106944
Received 27 March 2022; Received in revised form 24 November 2022; Accepted 4 December 2022
Available online 17 December 2022

volume granite intrusions (Černý, 1991a, b; Černý et al., 2012; London, 2008), has hampered the recognition of pegmatites as potentially linked to orogenic cycles. Recent findings showing that swarms of pegmatites can form by direct partial melting of metamorphic rocks (Fuchsloch et al., 2018; Konzett et al., 2018; Müller et al., 2015, 2017; Schuster et al., 2017; Simmons et al., 1996, 2016; Turlin et al., 2019; Webber et al., 2019) suggest that these anatectic events have regional character and might be important time markers of orogenic processes.

In this study, we provide a new set of ages of Sveconorwegian pegmatites (1) to compare their ages with those of adjacent granites, (2) to reveal temporal maxima of pegmatite formation and relate these to specific stages of the Sveconorwegian orogeny, (3) to test if different dating methods of different pegmatite minerals yield similar ages, and (4) to compare the data with those of the coeval Grenvillian orogeny.

The Sveconorwegian orogen hosts one of the largest pegmatite provinces in the world. >5000 large (>1000 $m^3$), granitic pegmatite bodies occur in seven pegmatite districts, each of which comprises several pegmatite fields (Fig. 1). The pegmatites consistently have Nb-Y-F (NYF) affinity, sit predominantly in amphibolites and amphibole-biotite gneisses, and are often associated with granites. Many of the pegmatites are, however, either older or younger than the adjacent granites or occur in areas with no exposed granites (Müller et al., 2015; 2017). The age difference, in addition to field observations, suggest no genetic relationship between pegmatites and granite. Instead, Müller et al. (2015, 2017) interpret these pegmatites to be of anatectic origin.

We test the genetic model proposed by Müller et al. (2015, 2017) by presenting additional age data in South Norway from previously dated pegmatite fields (Kragerø, Kristiansand and Østfold) and new age data for the Flesberg, Fyresdal, and Tørdal pegmatite fields together with a new age for the Tørdal granite. These new pegmatite and granite ages allow us to link the genesis of the pegmatites of southern Norway to various high-grade metamorphic stages of the Sveconorwegian orogeny. Finally we discuss, why the Sveconorwegian pegmatites have exclusively NYF affinity and there are no coeval pegmatites with Li-Cs-Ta (LCT) affinity although their protoliths, i.e., S-type granite gneisses and metasedimentary rocks, are common in the Sveconorwegian orogen.

## 2. Geological setting

### 2.1. Evolution of the Sveconorwegian orogen

The Sveconorwegian orogen covers southern Norway and southwestern Sweden (Fig. 1). The orogen formed between 1160 and 920 Ma (Bingen et al., 2008a, 2008b,2021; Falkum, 1985; Gower et al., 1990; Li et al., 2008; Möller and Andersson, 2018; Slagstad et al., 2017, 2020; Stephens and Wahlgren, 2020). It includes five lithotectonic units: The Eastern Segment and the Idefjorden, Kongsberg, Bamble, and Telemark lithotectonic units (Fig. 1; nomenclature according to the Geological Survey of Norway; Torgersen et al., 2021). The units were affected differently by the Sveconorwegian orogeny (Bingen et al., 2021; Slagstad et al., 2020) but all contain large (>1000 $m^3$) pegmatites. The main

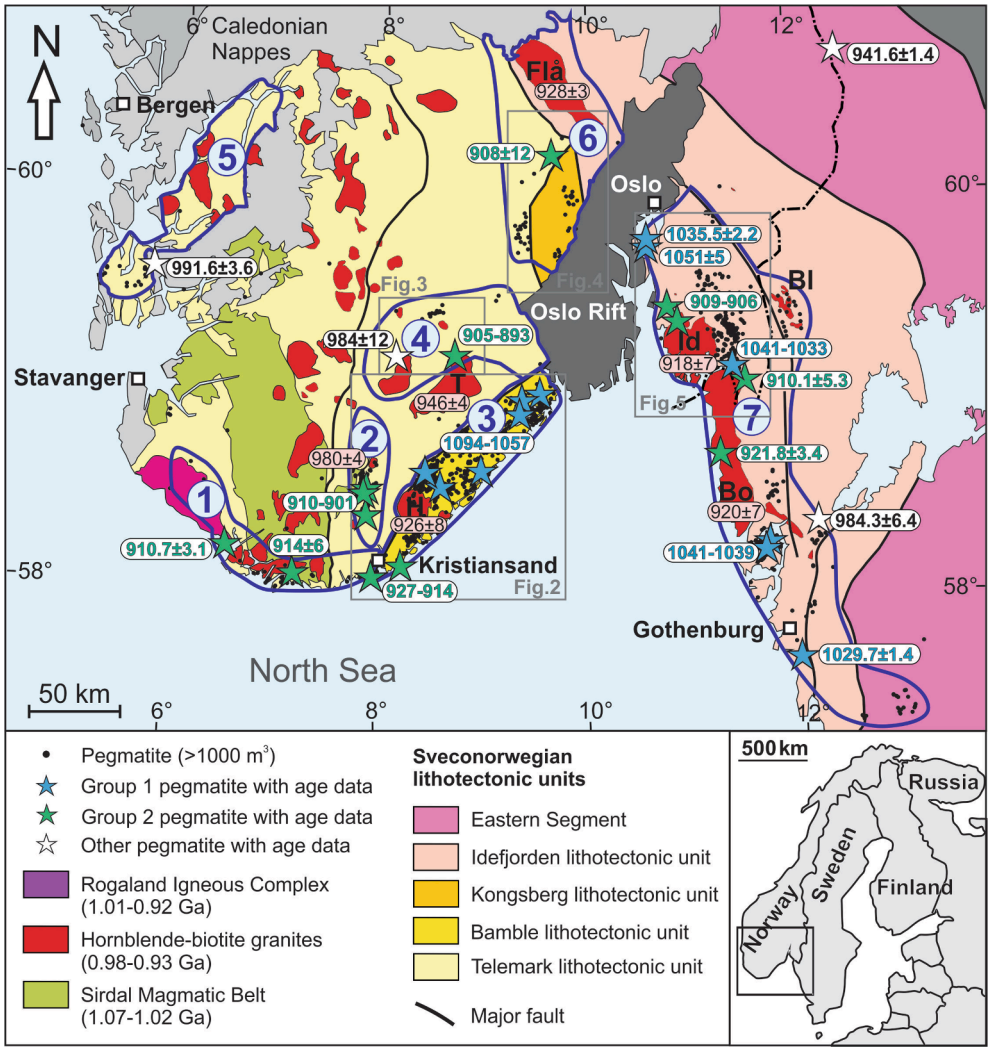


**Fig. 1.** Simplified geological map of the Sveconorwegian orogen showing the extent of the Sveconorwegian pegmatite province divided into seven pegmatite districts (solid blue line): 1 – Mandal, 2 – Setesdal, 3 – Bamble, 4 – Nissedal, 5 – Hardanger, 6 – Buskerud, 7 – Østfold-Halland. Post-orogenic granites: Bl – Blomskog granite, Bo – Bohus granite, Flå – Flå granite, H – Herefoss granite, Id – Iddefjord granite, T – Tørdal granite. Modified after Ihlen and Müller (2009). The map shows pegmatite (blue, green and black bold font) and granite (black normal font on pink background) ages obtained in this study and from the literature (Table 6). The pegmatites are divided into two age groups: Blue star = Group 1 pegmatites (1100–1030 Ma), green star = Group 2 pegmatites (930–890 Ma). (For interpretation of the references to colour in this figure legend, the reader is referred to the web version of this article.)

mineralogy and characteristics of the studied pegmatites are summarized in Table 1.

According to Bingen et al. (2008a) the Sveconorwegian orogeny comprised a series of four geographically and tectonically distinct events: the 1140–1080 Ma Arendal event, 1050–980 Ga Agder event (main compression phase), 980–970 Ma Falkenberg event (limited to the Eastern Segment), and 960–900 Ma Dalane event (extension and post-collisional magmatism). The period after ca. 1000 Ma was characterized by a shift from compressional to extensional tectonics in the western and central part of the orogen (Telemark, Bamble, Kongsberg and Idefjorden lithotectonic units) associated with the development of high heat flow due to widespread underplating by mafic magmas, recorded by LP-HT metamorphism and extensive granite emplacement (hornblende-biotite granite suite; Andersen et al., 2007b; Granseth et al., 2020).

In the following, we describe the magmatic and metamorphic events that coincide with pegmatite formation. The high-grade metamorphism in the Bamble lithotectonic unit at 1140–1080 Ma was followed by the emplacement of the 1060–1020 Ma granitic batholiths of the Sirdal Magmatic Belt in the Telemark lithotectonic unit (Coint et al., 2015). Voluminous basaltic underplating (Bybee et al., 2014; Slagstad et al., 2018) provided the heat source for large-scale crustal melting leading to the formation of the Sirdal Magmatic Belt (Coint et al., 2015). High-pressure (at c. 1045 Ma) and upper-amphibolite-facies metamorphism (at c. 1025 Ma) in the Idefjorden lithotectonic unit (Söderlund et al., 2008) coincided with the emplacement of the Sirdal Magmatic Belt. The last major magmatic event in the Sveconorwegian orogen occurred when the hornblende-biotite granite suite was emplaced 1000–920 Ma (Granseth et al., 2020; Høy,2016; Jensen and Corfu, 2016; Slagstad et al., 2013, 2018; Vander Auwera et al., 2003, 2011). The heat source for the hornblende-biotite granite magmatism is thought to be related to the underplating of mafic magmas due to crustal extension and mantle upwelling during this last orogenic stage (Andersen et al., 2007b; Granseth et al., 2020).

### 2.2. Sveconorwegian pegmatite districts

The Bamble pegmatite district contains several hundred large (>1000 $m^3$) pegmatite bodies intruded in an area of around 30 × 150 km stretching through the entire Bamble lithotectonic unit (Fig. 2). The district has the highest density of pegmatite occurrences in the Sveconorwegian pegmatite province (Müller et al., 2017) and comprises six pegmatite fields, from southwest to northeast the Kristiansand, Glamsland-Lillesand, Froland, Arendal, Søndeled, and Kragerø pegmatite fields (Fig. 2). Two hornblende-biotite granite plutons occur southwest of the Froland and Arendal fields: the Herefoss and the Grimstad granite with ages of 926 ± 8 Ma (Andersen, 1997) and 989 ± 8 Ma (Kullerud and Machado, 1991), respectively. We dated the Randesund and Salbostat pegmatites from the Kristiansand pegmatite field, and the Tangen, Bråten 2, Bjønndalen and Hullerøya 2 pegmatites from the Kragerø pegmatite field. Detailed information about the sampled pegmatites is provided in the Supplementary Material SM01.

*The Kristiansand pegmatite field* is located in the southernmost part of the Bamble lithotectonic unit. The field stretches 14 km NE-SW and is 4 km wide. It contains 12 abandoned feldspar quarries in pegmatites hosted by migmatitic gneiss and amphibolite. The pegmatites consist mainly of K-feldspar and quartz with minor beryl and columbite. One age exists for the Kristiansand pegmatite field; columbite from the Flekkerøy pegmatite yields an age of 915.4 ± 1.6 Ma (Müller et al., 2017).

*The Kragerø pegmatite field* contains about 70 large (>1000 $m^3$) pegmatites covering an area of 40 × 20 km. The pegmatites are hosted mainly by amphibolite but locally also by migmatitic amphibolite-biotite gneiss. They consist of K-feldspar, quartz, plagioclase, and biotite with accessory monazite, columbite, apatite, uraninite, allanite, zircon, magnetite, xenotime, and thorite. Columbite from the Tangen pegmatite yielded a U-Pb age of 1082.3 ± 4.5 Ma (Müller et al., 2017). In this study, we used a different sample than Müller et al. (2017) for dating of the Tangen pegmatite to test the robustness of the U-Pb

**Table 1**
Mineralogy of dated pegmatites.

| District | Field | Pegmatite | Major minerals | Common accessory minerals | Other characteristics |
|---|---|---|---|---|---|
| Bamble | Kragerø | Tangen | K-feldspar, albite, quartz | Biotite, magnetite, hematite, tourmaline, phenakite, allanite-(Ce), apatite, zircon, columbite group minerals, topaz | The dominant plagioclase is albite, mica (biotite) only found in the border zone |
| Bamble | Kragerø | Bråten 2 | Quartz, K-feldspar, plagioclase, biotite | Monazite-(Ce), apatite, uraninite | |
| Bamble | Kragerø | Hullerøya 2 | K-feldspar, quartz, biotite | Plagioclase, monazite-(Ce), allanite-(Ce), zircon, magnetite, xenotime-(Y), thorite | |
| Bamble | Kragerø | Bjønndalen | K-feldspar, plagioclase, quartz | Xenotime-(Y), monazite-(Ce), zircon, uraninite | |
| Bamble | Kristian-sand | Randesund | K-feldspar, albite, quartz, beryl | Garnet, muscovite, columbite group minerals, titanite, hematite, magnetite, fluorite, monazite-(Ce), gadolinite-(Y), molybdenite | |
| Bamble | Kristian-sand | Salbostat | K-feldspar, albite, quartz, beryl | Garnet, muscovite, columbite group minerals, titanite, hematite, magnetite, fluorite, monazite-(Ce), gadolinite-(Y), molybdenite | |
| Nissedal | Tørdal | Skardsfjell | 'Amazonite', quartz, albite | Polylithionite-sidrophyllite, muscovite, garnet, beryl, topaz, fluorite, ixiolite, cassiterite | Contains albite replacement zones |
| Nissedal | Tørdal | Upper Høydalen | K-feldspar, plagioclase, 'Amazonite', quartz, muscovite | Polylithionite-sidrophyllite, garnet, gadolinite-(Y), beryl, topaz, fluorite, ixiolite, cassiterite | Contains albite replacement zones |
| Nissedal | Fyresdal | Bjønnetjønn | K-feldspar, plagioclase, quartz, muscovite | Garnet, magnetite, monazite-(Ce) | |
| Østfold-Halland | Østfold | Herrebøkasa | K-feldspar, quartz, muscovite | Albite, garnet, monazite-(Ce), beryl, rutile, columbite group minerals, topaz, fluorite, uraninite, samarskite-(Y) | Contains one large cavity ca. 3 m in diameter, contains albite replacement zones |
| Østfold-Halland | Østfold | Halvorsrød | K-feldspar, plagioclase, muscovite | Biotite, albite, columbite group minerals, fluorite | Contains one large cavity ca. 2 m in diameter, contains albite replacement zones |
| Østfold-Halland | Østfold | Spro | K-feldspar, plagioclase, quartz, muscovite | Albite, tourmaline, beryl, columbite group minerals, topaz, fluorite, samarskite-(Y) | Weakly deformed, one of the very few tourmaline-bearing pegmatites |
| Buskerud | Flesberg | Bjertnes | K-feldspar, quartz, muscovite, biotite | Garnet, beryl, monazite-(Ce), xenotime-(Y), uraninite, molybdenite | Rich in monazite-(Ce) |

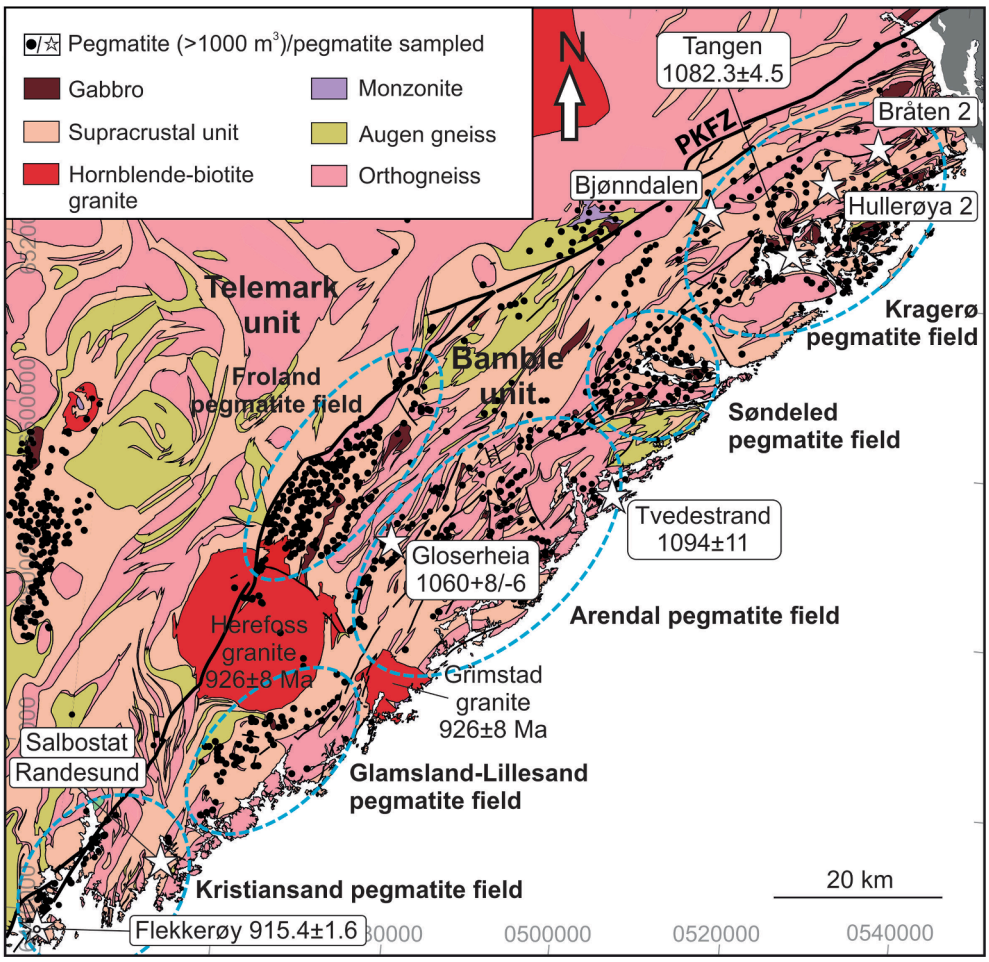


**Fig. 2.** Geological map of the Bamble pegmatite district including sample localities and pegmatite ages from the literature (Baadsgaard et al., 1984; Müller et al., 2017; Scherer et al., 2001). Porsgrunn-Kristiansand fault zone (PKFZ) marks the border between the Bamble and Telemark lithotectonic units. Modified after NGU 1:250.000 Geological map of Norway. Location of area is shown in Fig. 1.

columbite geochronometer.

The Nissedal pegmatite district is located in the Telemark lithotectonic unit. The district contains three pegmatite fields; the Kviteseid, Fyresdal and Tørdal fields (Fig. 3). All three pegmatite fields are hosted by metamorphic rocks of the Mesoproterozoic volcanic-sedimentary Nissedal supracrustal complex (Dons et al., 1960; Oftedahl, 1980). No published age data exist for these fields. We dated two pegmatites (Skardsfjell and Upper Høydalen) from Tørdal and one (Bjønnetjønn) from Fyresdal (see also Supplementary Material SM01).

*The Tørdal pegmatite field* consists of more than three hundred large (>1000 m$^3$) pegmatite bodies that occur north of the Tørdal-Treungen granite pluton. In addition, some chemical primitive pegmatites occur within the Tørdal granite. The Tørdal-Treungen granite is a large, possibly composite pluton and unusually rich in radioelements. Its emplacement age is not well-constrained, as the U-Pb zircon dates ranges from 918 ± 7 Ma (Andersen et al., 2007a) to 957 ± 12 Ma (Slagstad et al., 2018). Therefore, the Tørdal-Treungen granite is redated in this paper. The Tørdal pegmatite field shows chemical zonation on the regional scale, reflected in the distribution of pink, white and green K-feldspar (Segalstad and Raade, 2003). The zonation is not parallel to the pluton contact. The pegmatites are hosted by amphibolites and metagabbros belonging to the Nissedal supracrustal complex (Bergstøl and Juve, 1988; Oftedal, 1940). At the Kleppe quarry, located in the central part of the pegmatite field, field evidence suggests the pegmatites formed by *in situ* melting of amphibolite (see Fig. 3A in Steffenssen et al., 2020). Major minerals of Tørdal pegmatites comprise alkali feldspar, quartz, siderophyllite, oligoclase, muscovite, and albite (Rosing-Schow et al., 2018). Common accessory minerals are garnet, monazite, gadolinite, and allanite. The most evolved pegmatites in addition contain accessory polylithionite-trilithionite, polylithionite-siderophyllite, columbite, topaz, fluorite, cassiterite, and beryl (Bergstøl and Juve, 1988; Rosing-Schow et al., 2018). The pegmatites are known for their Sc enrichment (Bergstøl and Juve, 1988; Juve and Bergstøl, 1997; Steffenssen et al., 2020). The Skardsfjell and Upper Høydalen pegmatites, both dated in this study, represent the chemically most evolved pegmatites known from the Tørdal pegmatite field (Rosing-Schow et al., 2018).

*The Fyresdal pegmatite field* is relatively small (8 × 4 km) and contains c. 30 large pegmatites mainly hosted in amphibolite and biotite-gneiss. The pegmatite field occurs adjacent to the Fyresdal granite, with a poorly constrained age of 870 ± 50 Ma (Rb/Sr biotite age; Venugopal, 1970). K-feldspar, plagioclase, quartz, and muscovite dominate the pegmatites with minor monazite, magnetite and garnet. The investigated Bjønnetjønn pegmatite is 25 m wide, extends for 450 m and is hosted by amphibolite.

The Buskerud pegmatite district comprises pegmatites within the Kongsberg and Telemark lithotectonic units as well as within the northernmost part of the Idefjorden lithotectonic unit (Fig. 1). The Flesberg pegmatite field occurs in the Telemark lithotectonic unit and contains about 20 large pegmatites over an area of 60 × 16 km (Fig. 4). The investigated Bjertnes pegmatite consists mainly of K-feldspar, plagioclase, quartz, muscovite and biotite and is hosted by biotite-gneiss. Accessory minerals include beryl, chalcopyrite, spessartine, molybdenite, monazite, uraninite and xenotime. Uraninite has been

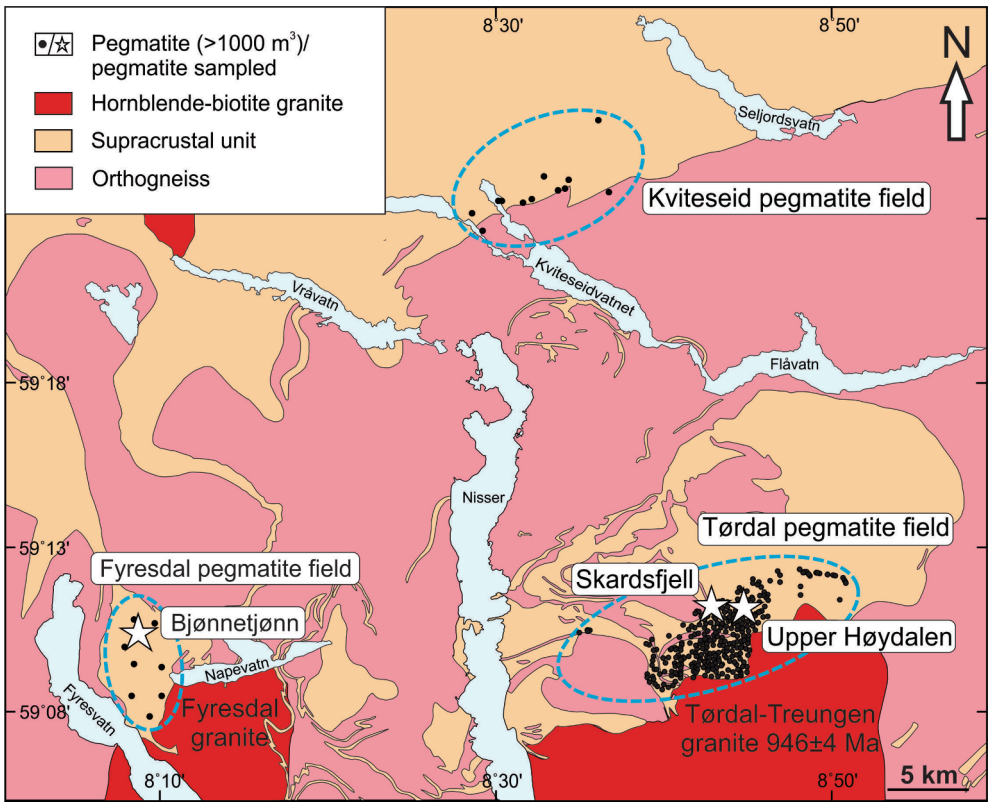


**Fig. 3.** Geological map of the Nissedal district with sample localities. Modified after NGU 1:250.000 Geological map of Norway. Location of the area is shown in Fig. 1.

dated to 950 ± 40 Ma (Bjørlykke and Burger, 1962).

The Østfold-Halland pegmatite district located within the Idefjorden lithotectonic unit is the largest of the seven Sveconorwegian districts stretching from Oslo to Gothenburg (Fig. 1). It includes>200 pegmatites mainly clustered adjacent to the Iddefjord and Bohus granites (Fig. 5). The two granites have similar ages: Dating of the Iddefjord granite gave ages of 918 ± 7 Ma (whole rock common Rb-Sr isochron age; Pedersen and Maaløe, 1990) and 928 ± 17 Ma (concordia U-Pb zircon age; Granseth et al., 2020), which is consistent with earlier dating of pegmatite dykes (U-Pb monazite age of 919 ± 5 Ma and U-Pb xenotime age of 922 ± 5 Ma) from within the Bohus granite in Sweden, the southern extension of the Iddefjord granite (Eliasson and Schöberg, 1991). The pegmatites surrounding the plutons define two major pegmatite fields, the Østfold and the Halland pegmatite fields. In this study we dated columbite from the Spro, Herrebøkasa, and Halvorsrød pegmatites of the Østfold pegmatite field (see also Supplementary Material SM01).

*The Østfold pegmatite field* situated in the northern part of the Idefjorden lithotectonic unit comprises approximately 150 large (>1000 $m^3$) pegmatite bodies and stretches approximately 80 km N—S between Oslo and Halden. The Iddefjord and the Bohus granite host some of the Østfold pegmatites, but most of them occur in amphibole-biotite gneisses. Müller et al. (2017) dated two pegmatites from the Østfold pegmatite field, the Karlshus pegmatite within the Iddefjord granite having a U-Pb columbite age of 906.3 ± 5.9 Ma and the Vintergruben pegmatite north of the granite with a crystallization age of 908.9 ± 1.4 Ma. The main minerals of the Østfold pegmatites are K-feldspar, plagioclase, quartz, biotite, and muscovite. The Iddefjord granite also hosts the Halvorsrød pegmatite investigated in this study. The pegmatite forms a flat dipping sheet with an amphibolite mega-enclave on top of it. The Herrebøkasa pegmatite sits at the contact between the Iddefjord granite and gneiss complex (Cooper et al., 2012). The Spro pegmatite forms an isolated body on the western shore of the Nesodden peninsula. No granite is exposed in vicinity of the pegmatite. The pegmatite sits on a regional N—S shear zone bordered by amphibolites and biotite gneisses.

## 3. Methods

### 3.1. Chemical microanalysis of the columbite group minerals and ixiolite

The complete sample list of all minerals used for age dating is provided in the Supplementary Material SM02. Pieces of columbite group minerals and ixiolite were mounted in one-inch epoxy casts, polished, and carbon coated. For the samples that had been annealed, both annealed and not annealed grains were mounted. The composition of the grains was determined using a CAMECA SX-100 Electron Probe Micro Analyzer (EPMA) at the Department of Geosciences, University of Oslo, Norway, using an accelerating voltage of 20 kV and a focused electron beam with a beam current of 20nA. Peak counting time was 20 s for Sn, Mn, and Ta and 30 s for Nb, Ti, Ca, Sc, Y, Th, U and Yb. The standard materials used for calibration included Nb, Ta, Fe—metals, Sn—$SnO_2$, Ti, Mn—pyrophanite, Ca—wollastonite, synthetic Y, Yb, Sc—orthophosphates (Jarosewich and Boatner, 1991), and Ca, Al, S—glasses with 15 wt% $ThO_2$ and $UO_2$, respectively. All elements were analysed in differential mode and background counting positions previously determined on detailed WDS scans. Correction of matrix effect and elemental interference were done using the PAP protocol (Pouchou and Pichoir, 1985). The calculation of the mineral formula bases on 6 anions for columbite group minerals and 8 anions for ixiolite.

### 3.2. ID-TIMS U-Pb analysis of columbite group minerals and ixiolite

U-Pb geochronological data were collected by Isotope Dilution Thermal Ionization Mass-Spectrometer (ID-TIMS) at the German Research Centre for Geosciences (GFZ) in Potsdam, Germany, on

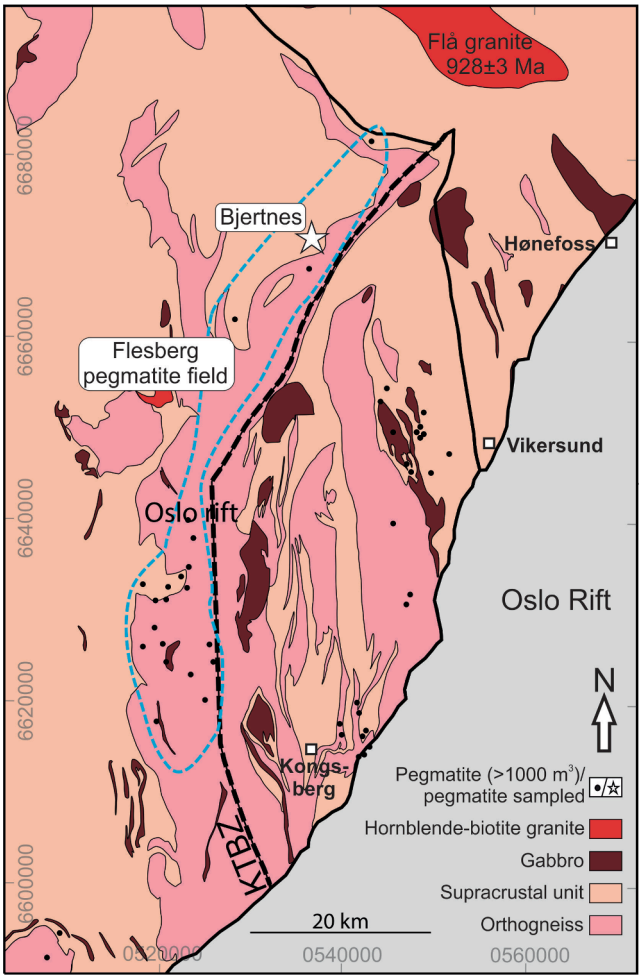


**Fig. 4.** Geological map of the Buskerud district with sample locality. Modified after NGU 1:250.000 Geological map of Norway. Location of the area is shown in Fig. 1. KTBZ – Kongsberg-Telemark boundary zone.

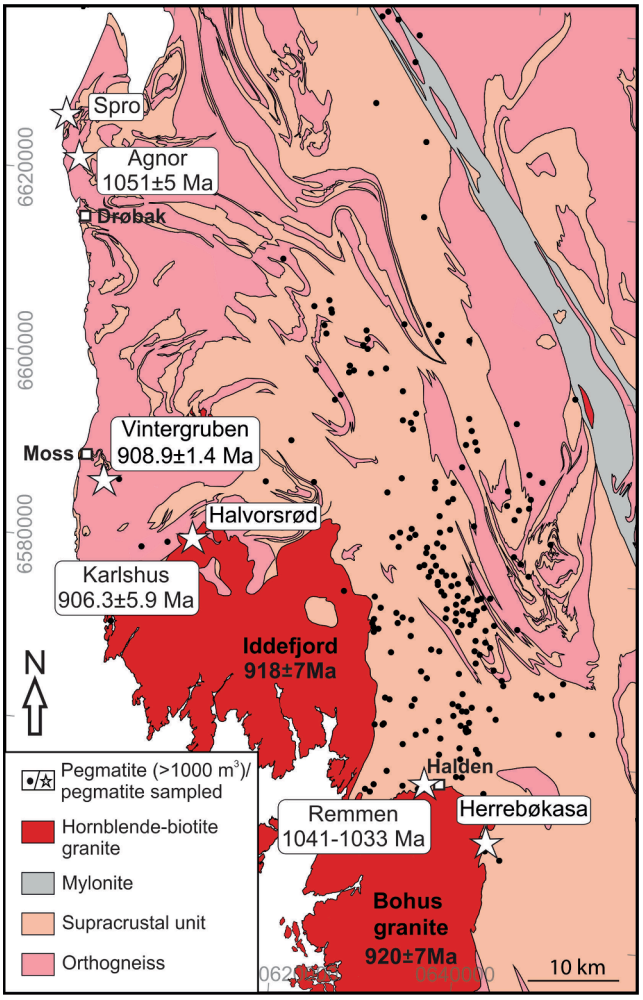


**Fig. 5.** Geological map of the Østfold-Halland pegmatite district including sample localities and pegmatite ages from the literature (Müller et al., 2017). Modified after NGU 1:250.000 Geological map of Norway and SGU 1:250.000 Geological map of Sweden. Location of area is shown in Fig. 1.

columbite group minerals and ixiolite. Columbite group minerals and ixiolite have been used for U-Pb dating of pegmatites as they may contain 500–1000 ppm U substituting into Fe and Mn sites in the crystal structure, whereas the substitution of $Pb^{2+}$ is not favoured (Romer and Wright, 1992). The decay of U induces damage in the crystal structure, which over time accumulates to a network of damages resulting in completely metamict minerals. Consequently, allowing for the migration of U and Pb and, thus, an open system behaviour of the U-Pb systems. Individual columbite crystals were broken into fragments. Crystalline columbite has a metallic lustre, which turns glassy with increased radiation damage. The least metamict parts were selected under the microscope. Three samples only had glassy fragments. These samples were annealed for an hour at 600 °C. All columbite samples were leached in 8 N HF at c. 70 °C to remove metamict domains that are exposed on grain surfaces. Complete removal of metamict domains will remove the disturbance of the U-Pb system and ideally results in concordant data (e.g. Romer and Smeds, 1996). Leaching by HF also removes readily dissolved inclusions that may host variable amounts of common Pb, such as sulphides and K-feldspar. Partial recrystallization of metamict domains, however, may partition U and Pb and result in a disturbed U-Pb system that after leaching yields normally or reversely discordant data. The corroded samples were then washed in 6 N HCl and 7 N $HNO_3$. Finally, the samples were washed with $H_2O$ and rinsed with acetone. Six fractions of each sample, consisting of one or several fragments, were selected for analysis. A mixed $^{205}Pb/^{235}U$ tracer and a droplet of $H_2SO_4$ were added to the samples before dissolution in HF overnight on a hot plate. After dissolution, the samples were dried, taken up in 3 N HCl, and loaded in Biorad® AG1-X8 ion-exchange resin to separate Pb and U, which were then loaded together on the same single re-filament except for the samples from Randesund, Salbostat, and Herrebøkasa. For these samples, Pb and U were loaded on separate single re-filaments. The Pb was measured at 1200–1260 °C and U at 1300–1400 °C.

### 3.3. EPMA U-Th-Pb dating of monazite

Monazite from six pegmatites (Bråten 2, Bjønndalen, Hullerøya 2, Bjertnes, Herrebøkasa, and Bjønnetjønn) was collected for dating. Monazite fragments of 2–6 mm diameter were mounted in epoxy and polished. The monazite composition was analysed using a CAMECA SX100 electron microprobe in wavelength-dispersion mode at the Joint Laboratory of Electron Microscopy and Microanalysis of the Masaryk University and Czech Geological Survey in Brno, Czech Republic. The analyses were done using 15 kV acceleration voltage, 200nA beam current, and 3 μm beam diameter. To optimise the detection limits peak counting times ranging from 20 to 240 s were used. Uranium was analysed on the U *M*β line with a counting time of 80 s and a detection limit of 200 ppm, Thorium was analysed on the Th *M*α line with a counting time of 60 s and a detection limit of 180 ppm, and Pb was analysed on the Pb*M*α line with a counting time of 240 s and a detection limit of 130

ppm. For standards, synthetic and natural phases were used: U—$UO_2$, Pb—vanadinite, Th—$CaTh(PO_4)_2$, P—$LaPO_4$, Y—YAG, La — $LaPO_4$, Ce — $CePO_4$, Pr — $PrPO_4$, Nd — $NdPO_4$, Sm— $SmPO_4$, Eu — $EuPO_4$, Gd — $GdPO_4$, Dy — $DyPO_4$, Er — $ErPO_4$, Ca, Si — wollastonite, Ca — $CaTh(PO_4)_2$, Fe — andradite, As—lammerite, Sr, S — $SrSO_4$, F — topaz). The data were reduced using the X-PHI matrix correction routine (Merlet 1994). Overlap of peaks and background positions were assessed and chosen using detailed WDS angle scans and natural and synthetic REE-phases. The background on Pb*M*α was modelled by exponential interpolation as described by Jercinovic and Williams (2005). In addition, Pb concentrations were manually corrected for Y*L*γ2, ThMζ1 and Th*M*ζ2 overlap on Pb*M*α. U concentrations were corrected for Th *M*γ overlap. The ages of the monazite samples were calculated using the method described by Montel et al. (1996).

### 3.4. ID-TIMS U-Pb analysis of zircon, Nb-Y-oxide and monazite

The ages of the Tørdal granite and the Upper Høydalen pegmatite were determined by the U-Pb method, by ID-TIMS at the Department of Geosciences of the University of Oslo. Zircon and Nb-Y-oxide grains were obtained using a Frantz vertical magnetic separator, heavy liquids, and a Frantz inclined magnetic separator. Zircon and Nb-Y-oxide grains were selected under a binocular microscope and zircon was air abraded to remove external disturbed domains (Davis et al., 1982; Krogh, 1982). Due to the metamict character of the Nb-Y-oxide grains it was not possible to obtain an X-ray diffraction pattern. The Nb-Y-oxide samples were not abraded. All chosen samples were washed with $HNO_3$, $H_2O$, and acetone, thereafter, weighed on a microbalance, and spiked with a mixed $^{202}Pb$-$^{205}Pb$-$^{235}U$ tracer. The zircon grains were dissolved with HF (+$HNO_3$) in Teflon bombs (Krogh, 1973) at 195 °C. As they were all ≤ 1 ug they were measured without chemical purification. The Nb-Y-minerals were dissolved in Savillex vials on a hot-plate using HF + $HNO_3$, dried, and re-dissolved in 6 N HCl. Prior to the chemical separation the solutions were evaporated and re-dissolved in 3 N HCl. The samples were processed through a single-stage HBr-HCl chemical separation (Corfu and Andersen, 2002). Monazite from the Upper Høydalen was dissolved in Savillex vials on a hot plate in 6 N HCl. The chemical separation for the monazite solutions was done with a two-stage procedure, purifying first the Pb with 1 N HBr, and in a second stage the U with 8 N $HNO_3$ and 6 N HCl. The samples were loaded on zone-refined Re filaments with Si-gel and $H_3PO_4$ and measured on a MAT 262 mass spectrometer either in static mode on Faraday cups or by peak-jumping using an ion-counting secondary electron multiplier. The data were corrected for 0.1 %/a.m.u fractionation using reproducibility factors of

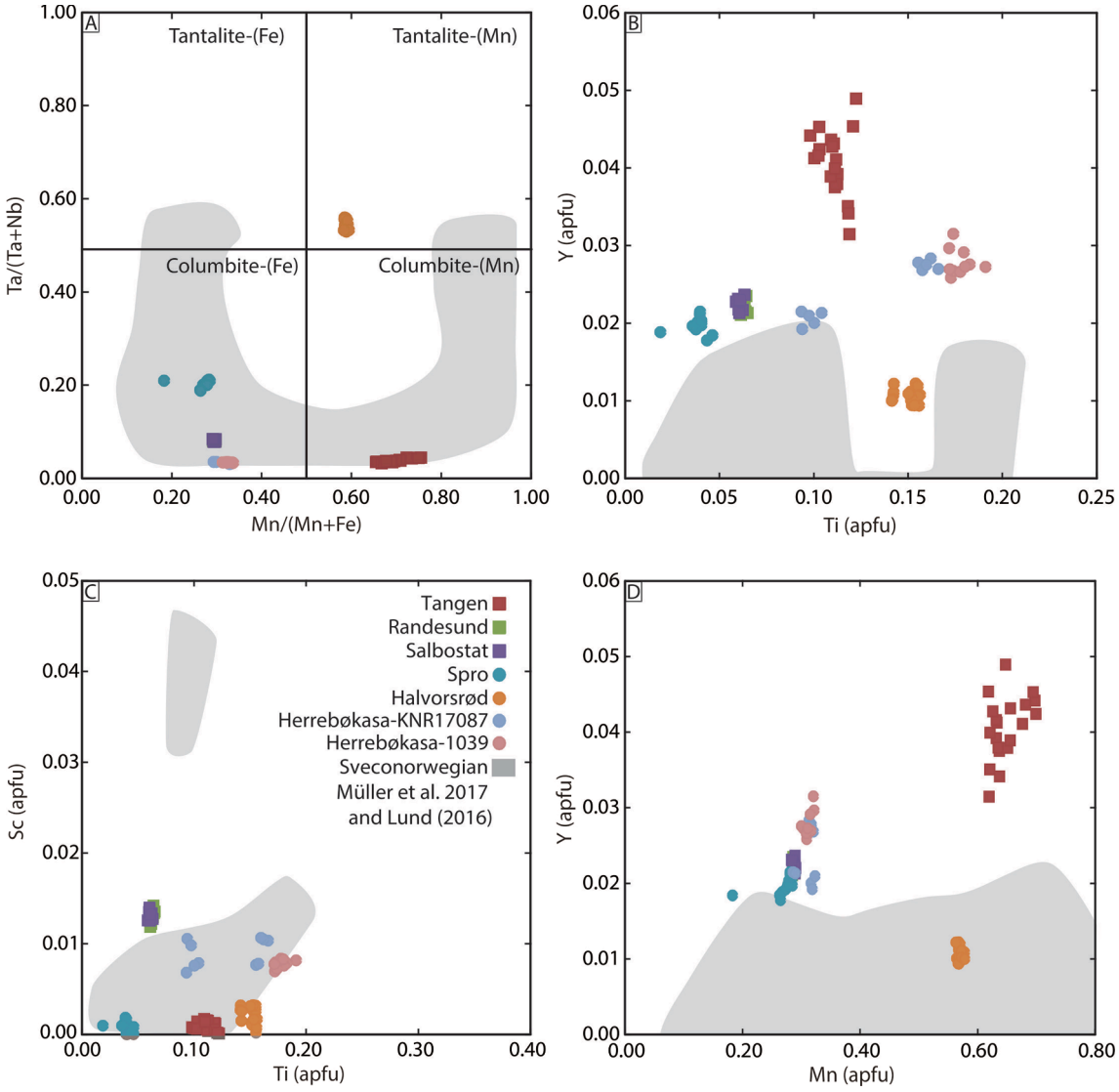


**Fig. 6.** Chemical composition of dated columbite group minerals. New data are provided in Supplementary Material SM03. Published data (grey fields) are from Müller et al. (2017), and Lund (2016). The chemical compositions of the Randesund and Salbostat columbite group minerals overlap in diagram A.

± 0.06 %/a.m.u. for the Faraday data and ± 0.1 %/a.m.u for the secondary electron multiplier data. The analyses were corrected for blanks of 2 pg Pb and 0.1 pg U. Residual initial common Pb was subtracted using compositions stated by Stacey and Kramers (1975). Decay constants of Jaffey et al. (1971) were used for the calculation of apparent ages. The data were reduced using the ROMAGE 5.1 program and were plotted in Isoplot (Ludwig, 1999).

## 4. Results

### 4.1. Chemistry of the columbite-group and ixiolite minerals

Ninety-four EPMA analyses were performed on six crystals. The EPMA results for columbite group minerals and ixiolite are listed in the Supplementary Material SM03. The data are plotted in Fig. 6A for classification. The samples from Halvorsrød and Tangen classify as tantalite-(Mn) and columbite-(Mn), respectively, whereas the samples from Randesund, Salbostat, Spro and Herrebøkasa all classify as columbite-(Fe). In the Sc vs Ti (apfu) diagram, data plot in two groups (Fig. 6C). Columbite-(Fe) from Randesund, Salbostat and Herrebøkasa has higher Sc and slightly higher Ti contents than columbite group minerals from Spro, Halvorsrød, and Tangen. Columbite from Tangen has high Mn and Y contents (Fig. 6B, D). Backscatter electron images of the dated columbite group minerals show that the grains are relatively homogenous. In contrast, backscatter electron images of ixiolite from Skardsfjell (Tørdal) show irregular zoning. The zoning, which is observed both in annealed and non-annealed grains, reflects within grain variation in Ta/(Nb + Ta).

### 4.2. Columbite-ixiolite U-Pb ID-TIMS ages of pegmatites

*Randesund* The six analysed fragments define a discordia line that intercepts the concordia at 918.1 ± 2.9 and 306 ± 180 (2σ; MSWD = 1.8). The discordia line is defined by three reversely discordant analyses and three normal discordant ones. Fragments that plot above the concordia may have experienced redistribution of U and Pb during their geological evolution leading to a loss of U relative to Pb. Little scatter is seen, but for one fragment (Randesund-5) with a slightly lower $^{207}Pb/^{206}Pb$ age (Table 2). The common Pb content is low (<0.6 pg). Randesund-2 has a higher U content (3067 ppm) than the other fragments (204.8–246.3 ppm U). The $^{232}Th/^{238}U$ ratios were calculated using the radiogenic Pb isotopic composition and the intercept age. The obtained values range from 0.02 to 0.03, which is distinctly higher than typically found in columbite group minerals (Romer and Smeds, 1994, 1996; Romer and Wright, 1992). We interpret the upper intercept at 918.1 ± 2.9 Ma (2σ) as the crystallization age of the Randesund pegmatite (Fig. 7A).

*Salbostat* Six columbite-(Fe) fragments from Salbostat define an upper intercept at 921.6 + 4.4/-5.1 Ma forcing the discordia line through 0 ± 200 Ma (2σ; MSWD = 2.0) (Fig. 7B). The samples are reversely discordant, except for one sample that is concordant (Salbostat-2). The discordance is interpreted to reflect incomplete removal of metamict domains by the acid-leaching procedure. All samples have similar U and Pb contents (Table 2). One fragment (Salbostat-1) has a markedly higher $^{232}Th/^{238}U$ ratio than the other fragments (Table 2), which may indicate that this fragment contained inclusions of a Th-rich mineral. The discordia line intercept of 921.6 + 4.4/-5.1 (2σ) is interpreted to date the crystallization age of the pegmatite at Salbostat.

*Herrebøkasa* Two columbite-(Fe) specimens from two different collections from Herrebøkasa were analysed (1039 and KNR17087). KNR17087 is a specimen from the collection of the Natural History Museum of Oslo, Norway. Six leached columbite-(Fe) fragments of sample 1039 yield reversely discordant data defining a discordia line with an upper intercept at 912.1 + 6.0/-7.7 Ma with the discordia line forced to 0 ± 200 Ma (2σ; MSWD = 1.16) (Fig. 7C). Most of the scatter derives from one fragment (Herrebøkasa-1) that has a slightly lower $^{207}Pb/^{206}Pb$ date than the others. Fragments of sample KNR17087, Herrebøkasa-7 to 10 and Herrebøkasa-12, are reversely discordant. Herrebøkasa-11 has only little U (10.87 ppm), which is uncommon for columbite group minerals, and is strongly reversely discordant. Therefore, it is not considered further. The Herrebøkasa-7, −8, −9, −10, and −12 fragments constrain a discordia line with much scatter that is mainly due to fragments Herrebøkasa-10 and Herrebøkasa-12. The KNR17087 contains numerous inclusions of euxenite-(Y), which could affect the dating. Forcing the discordia line through 0 ± 200 Ma gives an upper intercept at 908.1 ± 5.3 Ma (MSWD = 1.13) (Fig. 7D). The upper intercept ages for the two Herrebøkasa specimens overlap within uncertainties and supports the reliability of the applied method and justifies the use of collection specimens (see Supplementary Material SM02). This method and. Combining the data of the two crystals yields an upper intercept age of 910.1 ± 5.3 Ma (MSWD = 2.1; not illustrated in Fig. 7) for a discordia line ancored at 0 ± 200 Ma.

*Spro* The analyses of columbite-(Fe) from the Spro pegmatite are reversely discordant except for one sample (Spro-4; Table 2). The five fragments define a discordia line with an upper intercept of 1028 ± 34 Ma (2σ; MSWD = 3.3). Scatter is mainly caused by Spro-4 that is the only normal discordant sample and has the highest U content of 5335 ppm. Forcing the discordia through 0 Ma with a nominal error of 200 Ma reduces both the uncertainty of the upper intercept age and the MSWD. If Spro-4 is omitted and the line is forced through 0 Ma the upper intercept age is 1035.5 ± 2.2 Ma (2σ; MSWD = 0.96) (Fig. 7E), which we interpret as the crystallization age for the Spro pegmatite.

*Skardsfjell* Six fragments of ixiolite from Skardsfjell define a discordia line with an upper intercept age of 892.7 ± 8.8 Ma and a lower intercept at 43 ± 140 Ma (2σ; MSWD = 3.6) (Fig. 7F). We interpret the intercept age 892.7 ± 8.8 Ma (2σ) to be the crystallization age of the Skardsfjell pegmatite.

*Halvorsrød* The analysed fragments from Halvorsrød have unusual high U contents (2721–3043 ppm) and yield reversely and normally discordant data. They define a discordia line with an upper intercept at 902.9 ± 1.7 Ma and a lower intercept at 299 ± 130 Ma (2σ; MSWD = 0.52) (Fig. 7G). The upper intercept is considered as the crystallization age of the Halvorsrød pegmatite.

*Tangen* The Tangen columbite-(Mn) has unusual high $^{232}Th/^{238}U$ ratios ranging from 0.64 to 1.22, which are up to 100 times higher than in the other samples from this study. The reversely discordant fragments define a discordia line with an upper intercept of 1099 ± 20 Ma (2σ; MSWD = 34). Fragment Tangen-1 has high contents of U (278 ppm) and common Pb (3.2 ppm) compared to the other samples that have 63.3–96.5 ppm U and < 0.15 ppm $Pb_{common}$. Omitting fragment Tangen-1 from the regression yields an upper intercept of 1068 ± 29 and a lower intercept of 748 ± 220 Ma (2σ; MSWD = 2.2). Most of the scatter on this Discordia line comes from Tangen-2 that has the highest $^{232}Th/^{238}U$ ratio. A discordia without Tangen-1 and Tangen-2, forced through 0 Ma, yields an upper intercept of 1082.2 ± 4.8 (2σ; MSWD = 0.92) (Fig. 7H), which is interpreted as the pegmatite's crystallization age.

### 4.3. Monazite U-Th-Pb EPMA and U-Pb ID-TIMS ages

Monazite samples from six pegmatites were chosen for EPMA U-Th-Pb dating. The monazites all classify as monazite-(Ce) with similar chemistry (Table 3). Monazite may take up large amounts of Th commonly 3–15 wt%, but sometimes up to 25 wt% (Montel et al., 1996). It may also contain significant amounts of U, ranging from a few hundred ppm up to 5 wt% U (Montel et al., 1996). Precise chemical ages are only obtained for monazite with high contents of U and Th (Montel et al., 1996). The monazite-(Ce) samples from this study contain 9–18 wt % Th and 0.3–0.6 wt% U, concentrations which are high enough to provide chronological data of relative high precision. The calculated average ages for each for the analysed pegmatites are listed in Table 4.

*Herrebøkasa* The monazite from the Herrebøkasa pegmatite is

**Table 2**
U-Pb ID-TIMS columbite and ixiolite age data.

| Sample[a] | Weight (mg) | Concentrations (ppm) | | $^{206}Pb/^{204}Pb$ | Common lead (pg) | Radiogenic Pb (at%)[c] | | | Th/U[d] | Atomic ratios[c] | | | Apparent ages (Ma)[e] | | |
|---|---|---|---|---|---|---|---|---|---|---|---|---|---|---|---|
| | | U | Pb (tot) | Measured ratios[b] | Pb(tot)-Pb(rad) | $^{206}Pb$ | $^{207}Pb$ | $^{208}Pb$ | | $^{206}Pb/^{238}U$ | $^{207}Pb/^{235}U$ | $^{207}Pb/^{206}Pb$ | $^{206}Pb/^{238}U$ | $^{207}Pb/^{235}U$ | $^{207}Pb/^{206}Pb$ |
| **Randesund, Bamble** | | | | | | | | | | | | | | | |
| Randesund-1 | 0.101 | 226.4 | 33.1 | 2854 | 0.6 | 92.9 | 6.48 | 0.617 | 0.021 | 0.155 | 1.494 | 0.070 | 931 | 928 | 921 |
| Randesund-2 | 0.278 | 3067.0 | 32.2 | 15,409 | 0.1 | 92.9 | 6.48 | 0.614 | 0.021 | 0.156 | 1.495 | 0.070 | 73 | 105 | 921 |
| Randesund-3 | 0.093 | 226.6 | 32.8 | 8252 | 0.0 | 92.9 | 6.49 | 0.609 | 0.021 | 0.156 | 1.503 | 0.070 | 936 | 932 | 923 |
| Randesund-4 | 0.441 | 228.0 | 32.5 | 13,271 | 0.1 | 92.8 | 6.48 | 0.679 | 0.023 | 0.154 | 1.478 | 0.070 | 921 | 921 | 923 |
| Randesund-5 | 0.183 | 203.8 | 29.4 | 8157 | 0.1 | 92.8 | 6.45 | 0.747 | 0.025 | 0.155 | 1.486 | 0.069 | 930 | 925 | 912 |
| Randesund-6 | 0.269 | 246.3 | 34.9 | 14,867 | 0.1 | 92.8 | 6.47 | 0.693 | 0.023 | 0.153 | 1.467 | 0.070 | 916 | 917 | 918 |
| **Salbostat, Bamble** | | | | | | | | | | | | | | | |
| Salbostat-1 | 0.181 | 181.4 | 27.9 | 7344 | 0.2 | 87.2 | 6.08 | 6.74 | 0.242 | 0.155 | 1.489 | 0.070 | 928 | 926 | 920 |
| Salbostat-2 | 0.534 | 213.8 | 30.5 | 18,745 | 0.1 | 92.9 | 6.48 | 0.575 | 0.019 | 0.154 | 1.479 | 0.070 | 922 | 922 | 922 |
| Salbostat-3 | 0.443 | 253.1 | 36.1 | 13,481 | 0.1 | 93.0 | 6.49 | 0.531 | 0.018 | 0.154 | 1.481 | 0.070 | 922 | 923 | 923 |
| Salbostat-4 | 0.290 | 228.8 | 33.6 | 2432 | 0.8 | 92.9 | 6.48 | 0.576 | 0.019 | 0.155 | 1.489 | 0.070 | 928 | 926 | 922 |
| Salbostat-5 | 0.264 | 215.6 | 30.8 | 15,317 | 0.0 | 92.9 | 6.49 | 0.567 | 0.019 | 0.154 | 1.485 | 0.070 | 925 | 924 | 922 |
| Salbostat-6 | 0.191 | 206.0 | 29.5 | 6745 | 0.2 | 93.0 | 6.49 | 0.501 | 0.017 | 0.154 | 1.479 | 0.070 | 922 | 922 | 921 |
| **Herrebøkasa, Østfold (1039)** | | | | | | | | | | | | | | | |
| Herrebøkasa-1 | 0.064 | 278 | 41.3 | 3549 | 0.5 | 93.2 | 6.45 | 0.327 | 0.011 | 0.159 | 1.517 | 0.069 | 951 | 937 | 903 |
| Herrebøkasa-2 | 0.092 | 310 | 45.7 | 5480 | 0.4 | 93.1 | 6.47 | 0.442 | 0.015 | 0.158 | 1.519 | 0.070 | 948 | 937 | 914 |
| Herrebøkasa-3 | 0.123 | 374 | 53.7 | 5944 | 0.4 | 93.1 | 6.46 | 0.475 | 0.016 | 0.154 | 1.476 | 0.069 | 924 | 920 | 911 |
| Herrebøkasa-4 | 0.093 | 252 | 38.2 | 1730 | 1.2 | 93.1 | 6.48 | 0.394 | 0.013 | 0.159 | 1.523 | 0.070 | 949 | 939 | 916 |
| Herrebøkasa-5 | 0.174 | 267 | 39.2 | 6119 | 0.4 | 93.1 | 6.47 | 0.398 | 0.013 | 0.158 | 1.509 | 0.069 | 943 | 934 | 913 |
| Herrebøkasa-6 | 0.126 | 310 | 44.9 | 9718 | 0.2 | 93.1 | 6.67 | 0.433 | 0.015 | 0.156 | 1.496 | 0.069 | 936 | 929 | 912 |
| **Herrebøkasa, Østfold (KNR17087)** | | | | | | | | | | | | | | | |
| Herrebøkasa-7 | 0.081 | 216.0 | 26.9 | 934 | 1.6 | 93.2 | 6.46 | 0.297 | 0.010 | 0.161 | 1.544 | 0.069 | 964 | 948 | 909 |
| Herrebøkasa-8 | 0.084 | 161.6 | 23.8 | 3052 | 0.3 | 93.4 | 6.46 | 0.178 | 0.006 | 0.158 | 1.506 | 0.069 | 944 | 933 | 906 |
| Herrebøkasa-9 | 0.141 | 186.3 | 27.1 | 4172 | 0.3 | 93.3 | 6.47 | 0.213 | 0.007 | 0.156 | 1.491 | 0.069 | 935 | 927 | 909 |
| Herrebøkasa-10 | 0.066 | 169.8 | 25.7 | 1578 | 0.8 | 93.6 | 6.43 | 0.000 | 0.000 | 0.160 | 1.511 | 0.069 | 954 | 935 | 889 |
| Herrebøkasa-11 | 0.337 | 10.87 | 27.5 | 3609 | 0.4 | 93.4 | 6.47 | 0.138 | 0.005 | 4.010 | 38.33 | 0.069 | **** | 3728 | 908 |
| Herrebøkasa-12 | 0.166 | 167.3 | 24.9 | 3970 | 0.3 | 93.3 | 6.52 | 0.185 | 0.006 | 0.160 | 1.538 | 0.070 | 955 | 946 | 924 |
| **Spro, Nesodden, Østfold** | | | | | | | | | | | | | | | |
| Spro-1 | 0.253 | 107.0 | 18.0 | 2604 | 0.3 | 92.3 | 6.81 | 0.885 | 0.030 | 0.177 | 1.797 | 0.074 | 1048 | 1044 | 1035 |
| Spro-2 | 0.160 | 183.0 | 32.0 | 1329 | 1.4 | 92.2 | 6.80 | 1.010 | 0.034 | 0.179 | 1.816 | 0.074 | 1060 | 1051 | 1034 |
| Spro-3 | 0.226 | 128.0 | 21.1 | 4082 | 0.3 | 92.2 | 6.81 | 0.961 | 0.033 | 0.175 | 1.781 | 0.074 | 1040 | 1039 | 1036 |
| Spro-4 | 0.358 | 172.0 | 28.1 | 5355 | 0.3 | 92.2 | 6.80 | 0.966 | 0.033 | 0.174 | 1.768 | 0.074 | 1033 | 1034 | 1035 |
| Spro-5 | 0.364 | 51.20 | 8.80 | 1220 | 0.4 | 92.3 | 6.82 | 0.883 | 0.030 | 0.176 | 1.793 | 0.074 | 1045 | 1043 | 1038 |
| **Skardsfjell, Tørdal** | | | | | | | | | | | | | | | |
| Skardsfjell-1 | 0.026 | 685 | 104 | 807.7 | 6.6 | 93 | 6.42 | 0.586 | 0.020 | 0.154 | 1.465 | 0.069 | 922 | 916 | 900 |
| Skardsfjell-2 | 0.050 | 460 | 76.6 | 364.6 | 12 | 92.9 | 6.42 | 0.656 | 0.022 | 0.152 | 1.447 | 0.521 | 912 | 909 | 900 |
| Skardsfjell-3 | 0.106 | 653 | 114 | 277.1 | 22.7 | 93.1 | 6.41 | 0.445 | 0.015 | 0.152 | 1.438 | 0.069 | 910 | 905 | 894 |
| Skardsfjell-4 | 0.034 | 456 | 88.8 | 367.9 | 13.6 | 92.8 | 6.39 | 0.815 | 0.028 | 0.178 | 1.692 | 0.069 | 1056 | 1005 | 896 |
| Skardsfjell-5 | 0.108 | 482 | 76.4 | 453.6 | 9.9 | 93.6 | 6.43 | 0 | 0.000 | 0.150 | 1.421 | 0.069 | 902 | 898 | 888 |
| Skardsfjell-6 | 0.029 | 1046 | 178 | 267.3 | 36.5 | 93.2 | 6.39 | 0.419 | 0.014 | 0.147 | 1.386 | 0.870 | 881 | 883 | 886 |
| **Halvorsrød, Østfold** | | | | | | | | | | | | | | | |
| Halvorsrød-1 | 0.1 | 3043 | 424 | 36,054 | 0.8 | 92.8 | 6.42 | 0.802 | 0.027 | 0.150 | 1.431 | 0.069 | 902 | 902 | 903 |
| Halvorsrød-2 | 0.09 | 2686 | 389 | 607.4 | 8 | 92.8 | 6.43 | 0.805 | 0.027 | 0.153 | 1.462 | 0.050 | 918 | 915 | 907 |
| Halvorsrød-3 | 0.137 | 2776 | 392 | 27,193 | 1.2 | 92.8 | 6.42 | 0.783 | 0.026 | 0.152 | 1.450 | 0.069 | 912 | 910 | 905 |
| Halvorsrød-4 | 0.203 | 2926 | 397 | 30,353 | 1.1 | 92.8 | 6.42 | 0.777 | 0.026 | 0.149 | 1.419 | 0.069 | 894 | 897 | 905 |
| **Tangen, Bamble** | | | | | | | | | | | | | | | |
| Tangen-1 | 0.050 | 285.0 | 278 | 56 | 163.4 | 78.9 | 5.00 | 16.1 | 0.640 | 0.369 | 3.228 | 0.063 | 2026 | 1463 | 721 |

(*continued on next page*)

**Table 2** (*continued*)

| Sample[a] | Weight (mg) | Concentrations (ppm) | | $^{206}Pb/^{204}Pb$ | Common lead (pg) | Radiogenic Pb (at%)[c] | | | Th/U[d] | Atomic ratios[c] | | | Apparent ages (Ma)[e] | | |
|---|---|---|---|---|---|---|---|---|---|---|---|---|---|---|---|
| | | U | Pb (tot) | Measured ratios[b] | Pb(tot)-Pb(rad) | $^{206}Pb$ | $^{207}Pb$ | $^{208}Pb$ | | $^{206}Pb/^{238}U$ | $^{207}Pb/^{235}U$ | $^{207}Pb/^{206}Pb$ | $^{206}Pb/^{238}U$ | $^{207}Pb/^{235}U$ | $^{207}Pb/^{206}Pb$ |
| Tangen-2 | 0.117 | 392.7 | 96.5 | 8996 | 0.3 | 68.2 | 5.22 | 26.6 | 1.223 | 0.194 | 2.048 | 0.077 | 1142 | 1132 | 1112 |
| Tangen-3 | 0.059 | 375.0 | 87.3 | 4058 | 0.7 | 68.6 | 5.12 | 26.2 | 1.197 | 0.184 | 1.915 | 0.076 | 1088 | 1086 | 1084 |
| Tangen-4 | 0.184 | 297.8 | 66.8 | 4418 | 0.6 | 72.3 | 5.45 | 22.2 | 0.963 | 0.187 | 1.939 | 0.075 | 1103 | 1095 | 1078 |
| Tangen-5 | 0.102 | 284.7 | 79.2 | 239 | 15.1 | 74.7 | 5.61 | 19.7 | 0.827 | 0.197 | 2.039 | 0.075 | 1160 | 1129 | 1069 |
| Tangen-6 | 0.128 | 293.7 | 63.3 | 4338 | 0.6 | 74.9 | 5.66 | 19.5 | 0.816 | 0.187 | 1.953 | 0.076 | 1108 | 1100 | 1083 |

**a** Small fragments from single columbite grains. Fragments with fresh fracture surfaces were selected. All samples were leached in a mixture of 15–20 vol% HF and HBr before sample dissolution.
**b** Lead isotope ratios corrected for fractionation, blank and isotopic tracer. Samples were analyzed at GFZ German Research Centre for Geosciences, Potsdam, Germany, using a $^{205}Pb$-$^{235}U$ mixed isotopic tracer. During the measurement period, total blanks were<15 pg and 10 pg, resepctively, for lead and<1 pg for uranium.
**c** Lead corrected for fractionation, blank, isotopic tracer, and initial lead with the composition according to Stacey & Kramers (1975).
**d** The $^{232}Th/^{238}U$ ratio was calculated from radiogenic $^{208}Pb/^{206}Pb$ and the age of the sample.
**e** The apparent ages were calculated with the constants defined by Jaffey et al. (1971) recommended by IUGS. $\lambda_{238} = 1.55125$ E-10 $y^{-1}$, $\lambda_{235} = 9.848$ E-10 $y^{-1}$.

chemically homogenous with ca. 11 wt% Th and 0.4 wt% U. The age population shows some scatter but give a relatively precise age of 903.2 ± 9.5 Ma (MSWD = 0.76) based on 7 measurements. The age overlaps with the one determined by U-Pb ID-TIMS analysis of columbite.

*Bjønnetjønn* The highest Th contents (21 wt%) are found in the monazite specimen from the Bjønnetjønn pegmatite. Even though the analysed monazite is chemically homogeneous, some scatter is seen in the age population (MSWD = 1.7). The five measurements give an age of 984 ± 12 Ma.

*Bjertnes* Two monazite samples from the Bjertnes pegmatite were dated. The samples are chemically homogenous with Th and U contents of c. 11 wt% and c. 0.60 wt%, respectively. Some differences are seen in the ages of the two samples. One sample yields a chemical age of 908 ± 12 Ma (MSWD = 0.26) that bases on four analyses and omits one analysis with a distinctly lower age of 876.8 ± 23.9 Ma. The second monazite sample yields a age of 896 ± 18 Ma (MSWD = 1.4) based on five measurements. The two ages overlap within uncertainties. For further discussion, we use 908 ± 12 Ma as the crystallization age because that sample contains fewer micro inclusion and, thus, the result is are more reliable.

*Hullerøya 2* The Hullerøya 2 monazite is chemically homogenous with 15 wt% Th and 0.3 wt% U. The age population is homogenous (five measurements) giving an age of 1067 ± 10 Ma (MSWD = 0.6).

*Bråten 2* The Bråten 2 monazite sample is chemically homogenous with 14 wt% Th and 0.60 wt% U. The age population of five measurements yield an crystallization age of 1057 ± 10 Ma with a very low MSWD of 0.12.

*Bjønndalen* The Bjønndalen monazite sample has a homogenous age population (five measurements) resulting in an age of 1064 ± 10 Ma (MSWD = 0.37). The sample is also chemically homogenous.

*Upper Høydalen* U-Pb ID-TIMS dates of three monazite grains from the Upper Høydalen pegmatite overlap within analytical uncertainties. They all plot above the concordia diagram because of excess $^{206}Pb$, which derives from $^{230}Th$ and is a common feature in minerals with high Th/U ratio, such as monazite or allanite (Schärer, 1984). As the $^{207}Pb/^{235}U$ is not affected by initial disequilibrium in the decay series, the mean $^{207}Pb/^{235}U$ age of 905.0 ± 2.4 Ma (MSWD = 1.6) is the best age estimate for monazite crystallization (Fig. 8; Table 5).

### 4.4. Zircon and Nb-Y-oxide U-Pb ID-TIMS age of the Tørdal-Treungen granite

The emplacement age of the Tørdal-Treungen granite was estimated by means of U-Pb ID-TIMS data on zircon and Nb-Y-oxide from a sample in the northeastern part of the granite pluton, in Tørdal. Three zircon grains and four grains of an unidentified Nb-Y-oxide were analysed (Table 5).The zircon grains contain U- and Th-rich inclusions and are metamict. Zircon and Nb-Y-oxide data were used to define a discordia line with an upper intercept at 946 ± 4 Ma and a lower intercept at 383 ± 10 Ma (2σ; MSWD = 2.8) (Fig. 9). The analyses are discordant and most of them cluster close to the upper intercept. As opposed to the pegmatite analyses all the granite analyses are normal discordant. The Nb-Y-oxide is very rich in common Pb and U compared to the zircons and has higher $^{232}Th/^{238}U$ ratios. We consider the upper intercept age of 946 ± 4 Ma a good estimate for the crystallization age of the sample of the Tørdal granite.

## 5. Discussion

### 5.1. Definition of pegmatite age groups and their implications for Sveconorwegian orogeny

Based on our new comprehensive age data set and previously published data we distinguish the Sveconorwegian pegmatites (>1000 $m^3$) into two major age groups; Group 1: 1100–1030 Ma and Group 2: 930–890 Ma (Table 6). Out of 32 pegmatite ages, 11 fall into Group 1

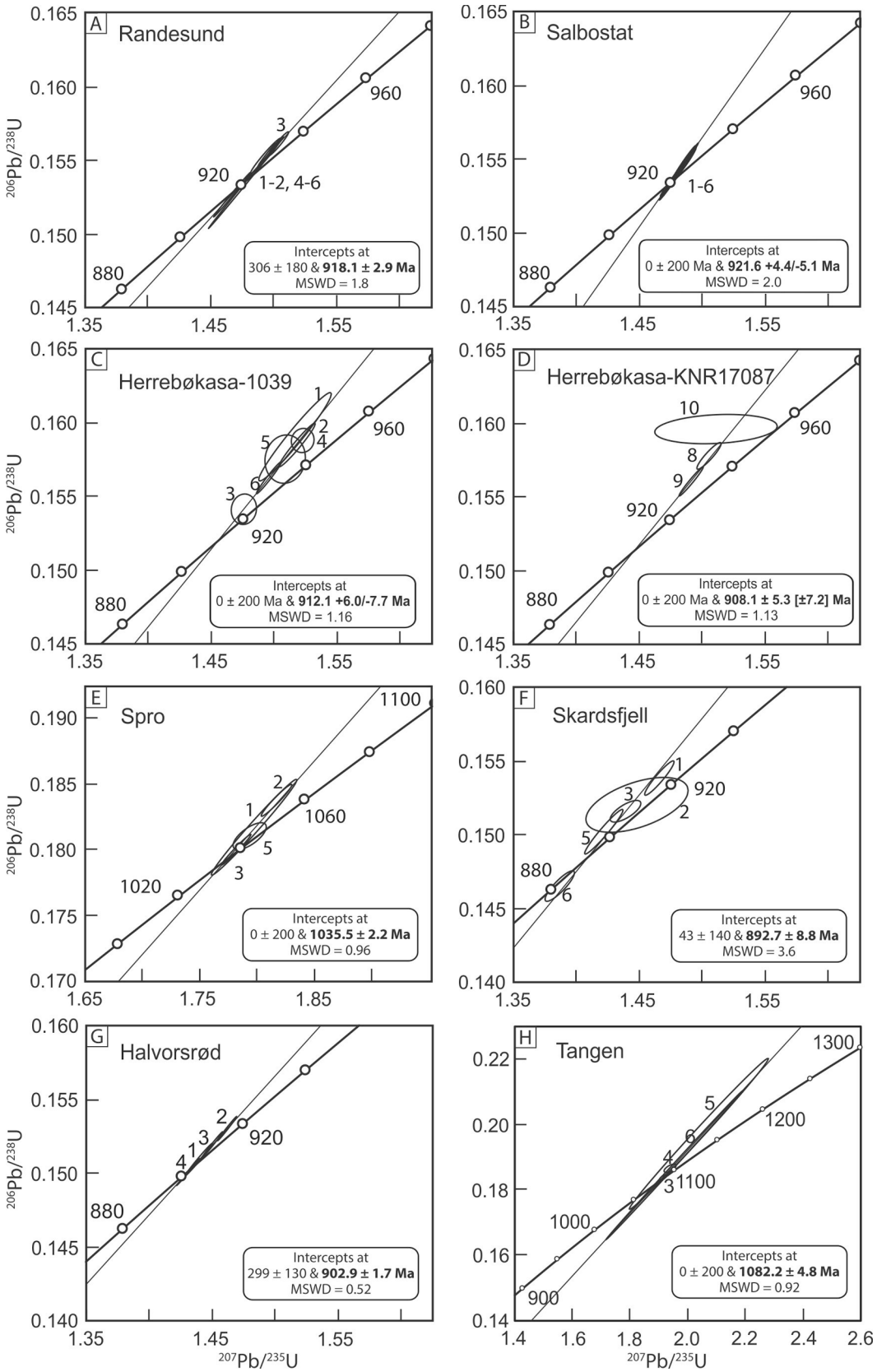


**Fig. 7.** Concordia diagrams showing U-Pb ID-TIMS data for columbite group minerals and ixiolite from the Randesund, Salbostat, Herrebøkasa-1039, Herrebøkasa-KNR17087, Spro, Skardsfjell, Halvorsrød, and Tangen pegmatites. The small numbers correspond to analysis numbers in Table 2.

**Table 3**
Monazite EPMA analyses and calculated age data.

| Sample | Herrebøkasa, Østfold | | | | | | | Bjønnetjønn, Tørdal | | | | | | Hullerøya 2, Bamble | | | |
|---|---|---|---|---|---|---|---|---|---|---|---|---|---|---|---|---|---|
| Age Ma | 894 | 914 | 910 | 917 | 899 | 901 | 886 | 978 | 992 | 996 | 964 | 984 | 991 | 1066 | 1075 | 1070 | 1052 |
| Age err Ma (2σ) | 26 | 26 | 25 | 26 | 26 | 26 | 26 | 18 | 18 | 18 | 18 | 18 | 18 | 23 | 23 | 23 | 23 |
| Th* | 10.83 | 10.87 | 10.89 | 10.84 | 10.74 | 10.55 | 10.62 | 19.39 | 19.45 | 19.30 | 19.31 | 19.42 | 19.50 | 13.67 | 13.75 | 13.87 | 13.86 |
| Pb korr | 0.44 | 0.45 | 0.45 | 0.45 | 0.44 | 0.43 | 0.43 | 0.87 | 0.88 | 0.88 | 0.85 | 0.87 | 0.88 | 0.67 | 0.68 | 0.68 | 0.67 |
| U korr | 0.37 | 0.37 | 0.38 | 0.38 | 0.38 | 0.37 | 0.36 | 0.47 | 0.48 | 0.47 | 0.46 | 0.47 | 0.46 | 0.27 | 0.27 | 0.27 | 0.26 |
| $Y_2O_3$ | 2.34 | 2.35 | 2.36 | 2.35 | 2.34 | 2.36 | 2.33 | 2.27 | 2.27 | 2.25 | 2.24 | 2.26 | 2.29 | 3.26 | 3.28 | 3.23 | 3.20 |
| $SiO_2$ | 1.96 | 1.96 | 1.96 | 1.96 | 1.92 | 1.89 | 1.92 | 5.15 | 5.19 | 5.13 | 5.17 | 5.20 | 5.15 | 2.36 | 2.39 | 2.43 | 2.44 |
| SrO | <0.01 | <0.01 | <0.01 | <0.01 | <0.01 | <0.01 | <0.01 | <0.01 | <0.01 | <0.01 | <0.01 | <0.01 | <0.01 | <0.01 | <0.01 | <0.01 | <0.01 |
| $P_2O_5$ | 27.14 | 27.30 | 27.33 | 27.35 | 27.48 | 27.62 | 27.29 | 21.86 | 21.94 | 21.73 | 21.73 | 22.00 | 21.91 | 26.27 | 26.47 | 26.13 | 26.34 |
| $Pr_2O_3$ | 2.89 | 2.88 | 2.83 | 2.86 | 2.90 | 2.93 | 2.86 | 2.92 | 2.84 | 2.86 | 2.92 | 2.86 | 2.93 | 2.55 | 2.61 | 2.56 | 2.58 |
| CaO | 0.80 | 0.79 | 0.81 | 0.81 | 0.79 | 0.79 | 0.79 | 0.10 | 0.11 | 0.11 | 0.13 | 0.11 | 0.09 | 1.48 | 1.48 | 1.47 | 1.45 |
| $ThO_2$ | 10.99 | 11.05 | 11.01 | 10.97 | 10.85 | 10.65 | 10.78 | 20.35 | 20.41 | 20.29 | 20.32 | 20.40 | 20.52 | 14.59 | 14.67 | 14.81 | 14.82 |
| $UO_2$ | 0.42 | 0.42 | 0.43 | 0.43 | 0.43 | 0.42 | 0.41 | 0.54 | 0.54 | 0.53 | 0.52 | 0.53 | 0.52 | 0.31 | 0.31 | 0.31 | 0.30 |
| $La_2O_3$ | 11.40 | 11.48 | 11.45 | 11.44 | 11.44 | 11.47 | 11.50 | 6.68 | 6.73 | 6.62 | 6.68 | 6.70 | 6.66 | 10.55 | 10.65 | 10.64 | 10.69 |
| $Ce_2O_3$ | 25.42 | 25.34 | 25.34 | 25.43 | 25.37 | 25.67 | 25.57 | 19.37 | 19.30 | 19.18 | 19.21 | 19.29 | 19.30 | 20.94 | 20.92 | 20.99 | 20.97 |
| $Nd_2O_3$ | 10.28 | 10.32 | 10.25 | 10.25 | 10.23 | 10.36 | 10.29 | 12.90 | 12.93 | 12.80 | 12.83 | 12.81 | 12.89 | 10.35 | 10.36 | 10.21 | 10.29 |
| $As_2O_5$ | <0.01 | <0.01 | <0.01 | <0.01 | <0.01 | <0.01 | <0.01 | <0.01 | <0.01 | <0.01 | <0.01 | <0.01 | <0.01 | <0.01 | <0.01 | <0.01 | <0.01 |
| FeO | <0.01 | <0.01 | <0.01 | <0.01 | <0.01 | <0.01 | <0.01 | <0.01 | <0.01 | <0.01 | <0.01 | <0.01 | <0.01 | <0.01 | <0.01 | <0.01 | <0.01 |
| $Sm_2O_3$ | 1.93 | 1.92 | 2.01 | 1.98 | 1.89 | 1.99 | 1.99 | 3.32 | 3.30 | 3.24 | 3.20 | 3.35 | 3.28 | 2.46 | 2.35 | 2.35 | 2.43 |
| $Eu_2O_3$ | <0.01 | 0.03 | 0.02 | 0.07 | 0.02 | <0.01 | 0.02 | <0.01 | <0.01 | <0.01 | <0.01 | <0.01 | <0.01 | 0.09 | 0.11 | 0.07 | 0.05 |
| $Gd_2O_3$ | 1.32 | 1.36 | 1.34 | 1.34 | 1.34 | 1.37 | 1.38 | 1.91 | 1.89 | 1.87 | 2.01 | 1.87 | 1.93 | 2.14 | 2.03 | 2.07 | 2.02 |
| $Dy_2O_3$ | 0.64 | 0.64 | 0.66 | 0.61 | 0.62 | 0.63 | 0.63 | 0.58 | 0.61 | 0.62 | 0.65 | 0.63 | 0.58 | 0.90 | 0.82 | 0.89 | 0.86 |
| $Er_2O_3$ | 0.16 | 0.16 | 0.15 | 0.19 | 0.18 | 0.15 | 0.17 | 0.10 | 0.11 | 0.11 | 0.13 | 0.11 | 0.12 | 0.27 | 0.25 | 0.27 | 0.22 |
| $SO_3$ | <0.02 | <0.02 | <0.02 | <0.02 | <0.02 | <0.02 | <0.02 | 0.04 | 0.05 | 0.07 | 0.06 | 0.03 | 0.03 | 0.14 | 0.14 | 0.15 | 0.16 |
| PbO | 0.48 | 0.49 | 0.49 | 0.49 | 0.48 | 0.47 | 0.46 | 0.93 | 0.95 | 0.95 | 0.92 | 0.94 | 0.95 | 0.72 | 0.73 | 0.73 | 0.72 |
| Total | 98.15 | 98.48 | 98.44 | 98.52 | 98.26 | 98.76 | 98.39 | 99.01 | 99.16 | 98.35 | 98.69 | 99.09 | 99.14 | 99.36 | 99.56 | 99.29 | 99.52 |
| Apfu | Based on 4 oxygens | | | | | | | | | | | | | | | | |
| Ce | 0.38 | 0.37 | 0.37 | 0.37 | 0.37 | 0.38 | 0.38 | 0.30 | 0.30 | 0.30 | 0.30 | 0.30 | 0.30 | 0.31 | 0.31 | 0.31 | 0.31 |
| Nd | 0.15 | 0.15 | 0.15 | 0.15 | 0.15 | 0.15 | 0.15 | 0.20 | 0.20 | 0.20 | 0.20 | 0.19 | 0.20 | 0.15 | 0.15 | 0.15 | 0.15 |
| La | 0.17 | 0.17 | 0.17 | 0.17 | 0.17 | 0.17 | 0.17 | 0.10 | 0.11 | 0.10 | 0.11 | 0.10 | 0.10 | 0.16 | 0.16 | 0.16 | 0.16 |
| Y | 0.05 | 0.05 | 0.05 | 0.05 | 0.05 | 0.05 | 0.05 | 0.05 | 0.05 | 0.05 | 0.05 | 0.05 | 0.05 | 0.07 | 0.07 | 0.07 | 0.07 |
| Th | 0.10 | 0.10 | 0.10 | 0.10 | 0.10 | 0.10 | 0.10 | 0.20 | 0.20 | 0.20 | 0.20 | 0.20 | 0.20 | 0.13 | 0.13 | 0.14 | 0.14 |
| U | 0.00 | 0.00 | 0.00 | 0.00 | 0.00 | 0.00 | 0.00 | 0.01 | 0.01 | 0.01 | 0.00 | 0.00 | 0.00 | 0.00 | 0.00 | 0.00 | 0.00 |
| Sr | 0.00 | 0.00 | 0.00 | 0.00 | 0.00 | 0.00 | 0.00 | 0.00 | 0.00 | 0.00 | 0.00 | 0.00 | 0.00 | 0.00 | 0.00 | 0.00 | 0.00 |
| Ca | 0.03 | 0.03 | 0.03 | 0.03 | 0.03 | 0.03 | 0.03 | 0.00 | 0.00 | 0.00 | 0.01 | 0.01 | 0.00 | 0.06 | 0.06 | 0.06 | 0.06 |
| Fe | 0.00 | 0.00 | 0.00 | 0.00 | 0.00 | 0.00 | 0.00 | 0.00 | 0.00 | 0.00 | 0.00 | 0.00 | 0.00 | 0.00 | 0.00 | 0.00 | 0.00 |
| Pb | 0.01 | 0.01 | 0.01 | 0.01 | 0.01 | 0.01 | 0.01 | 0.01 | 0.01 | 0.01 | 0.01 | 0.01 | 0.01 | 0.01 | 0.01 | 0.01 | 0.01 |
| Pr | 0.04 | 0.04 | 0.04 | 0.04 | 0.04 | 0.04 | 0.04 | 0.05 | 0.04 | 0.04 | 0.05 | 0.04 | 0.05 | 0.04 | 0.04 | 0.04 | 0.04 |
| Sm | 0.03 | 0.03 | 0.03 | 0.03 | 0.03 | 0.03 | 0.03 | 0.05 | 0.05 | 0.05 | 0.05 | 0.05 | 0.05 | 0.03 | 0.03 | 0.03 | 0.03 |
| Eu | 0.00 | 0.00 | 0.00 | 0.00 | 0.00 | 0.00 | 0.00 | 0.00 | 0.00 | 0.00 | 0.00 | 0.00 | 0.00 | 0.00 | 0.00 | 0.00 | 0.00 |
| Gd | 0.02 | 0.02 | 0.02 | 0.02 | 0.02 | 0.02 | 0.02 | 0.03 | 0.03 | 0.03 | 0.03 | 0.03 | 0.03 | 0.03 | 0.03 | 0.03 | 0.03 |
| Dy | 0.01 | 0.01 | 0.01 | 0.01 | 0.01 | 0.01 | 0.01 | 0.01 | 0.01 | 0.01 | 0.01 | 0.01 | 0.01 | 0.01 | 0.01 | 0.01 | 0.01 |
| Er | 0.00 | 0.00 | 0.00 | 0.00 | 0.00 | 0.00 | 0.00 | 0.00 | 0.00 | 0.00 | 0.00 | 0.00 | 0.00 | 0.00 | 0.00 | 0.00 | 0.00 |
| Sum A | 0.99 | 0.99 | 0.99 | 0.99 | 0.98 | 0.98 | 0.99 | 1.00 | 1.00 | 1.00 | 1.00 | 0.99 | 1.00 | 1.01 | 1.01 | 1.01 | 1.01 |
| P | 0.93 | 0.93 | 0.93 | 0.93 | 0.94 | 0.94 | 0.93 | 0.79 | 0.79 | 0.79 | 0.78 | 0.79 | 0.79 | 0.90 | 0.90 | 0.90 | 0.90 |
| Si | 0.08 | 0.08 | 0.08 | 0.08 | 0.08 | 0.08 | 0.08 | 0.22 | 0.22 | 0.22 | 0.22 | 0.22 | 0.22 | 0.10 | 0.10 | 0.10 | 0.10 |
| As | 0.00 | 0.00 | 0.00 | 0.00 | 0.00 | 0.00 | 0.00 | 0.00 | 0.00 | 0.00 | 0.00 | 0.00 | 0.00 | 0.00 | 0.00 | 0.00 | 0.00 |
| S | 0.00 | 0.00 | 0.00 | 0.00 | 0.00 | 0.00 | 0.00 | 0.00 | 0.00 | 0.00 | 0.00 | 0.00 | 0.00 | 0.00 | 0.00 | 0.00 | 0.00 |
| Sum B | 1.01 | 1.01 | 1.01 | 1.01 | 1.01 | 1.01 | 1.01 | 1.01 | 1.01 | 1.01 | 1.01 | 1.01 | 1.01 | 1.00 | 1.00 | 1.00 | 1.00 |

and 17 fall into Group 2. Four pegmatite ages do not fall into either group: the Riddaho pegmatite (941.6 ± 1.4 Ma; Romer and Smeds, 1996), the Skuleboda pegmatite (984.3 ± 6.4 Ma; Romer and Smeds, 1996), the Tors gruve pegmatite (991.6 ± 3.6 Ma; Müller et al., 2017), and the Bjønnetjønn pegmatite (984 ± 12 Ma; Table 4). These four pegmatites occur in the different parts of the Sveconorwegian orogen (Fig. 1). The Riddaho, Skuleboda, and Tors gruve pegmatites have in common that they occur as isolated bodies. The Bjønnetjønn pegmatite is part of the Fyresdal pegmatite field, a small field of about 10 large bodies located in the central Telemark lithotectonic unit. The pegmatites are coeval with but spatially unrelated to some granitic intrusions, such as the Finse batholith (985.6 ± 1.6 Ma, Jensen and Corfu 2016), which combined with their location suggests that these pegmatites represent isolated melting events (see Müller et al., 2017).

Pegmatites of the two age groups do not only differ in age but also in magmatic texture and mineralogy, essentially reflecting different degrees of fractionation and/or chemically differently evolved melts, and indirectly also indicating different settings of formation. The differences between Group 1 and 2 pegmatites are summarized in Table 7. Most importantly, Group 2 pegmatites are more evolved than Group 1 pegmatites. Group 2 pegmatites generally have a better developed mineralogical zoning and their mineral compositions support the notion of representing more differentiated melts: 'Amazonite' is much more common in Group 2 and mica and columbite group mineral compositions, for example, are more evolved than in Group 1 pegmatites (Rosing-Schow et al. 2018). Columbite group minerals of Group 2 pegmatites exhibit a broad range of Ta/(Ta + Nb) and Mn/(Mn + Fe) ratios reaching more evolved compositions than columbite group minerals of Group 1 pegmatites (Fig. 10).

### 5.1.1. *Tectonic setting of Group 1 pegmatites (1100–1030 Ma)*

Group 1 pegmatites in the *Bamble lithotectonic unit* are spread throughout the unit with ages ranging from 1094 to 1060 Ma. The four new ages presented here were determined on pegmatites from the Kragerø pegmatite field in the NE end of the Bamble unit. These data together with published crystallization ages from Froland (Baadsgaard

| Hullerøya 2, Bamble | Bjertnes A, Buskerud | | | | | Bjertnes B, Buskerud | | | | | Bråten 2, Bamble | | | | | Bjønndalen, Bamble | | | | |
|---|---|---|---|---|---|---|---|---|---|---|---|---|---|---|---|---|---|---|---|---|
| 1070 | 905 | 877 | 908 | 904 | 917 | 876 | 901 | 888 | 914 | 901 | 1063 | 1057 | 1054 | 1057 | 1053 | 1075 | 1055 | 1061 | 1066 | 1064 |
| 23 | 24 | 24 | 24 | 24 | 24 | 24 | 24 | 24 | 24 | 24 | 23 | 24 | 24 | 24 | 23 | 23 | 23 | 23 | 23 | 23 |
| 13.85 | 11.60 | 11.61 | 11.57 | 11.53 | 11.51 | 11.41 | 11.39 | 11.33 | 11.36 | 11.40 | 13.70 | 13.54 | 13.56 | 13.58 | 13.68 | 13.67 | 13.81 | 13.77 | 13.75 | 13.76 |
| 0.68 | 0.48 | 0.47 | 0.48 | 0.48 | 0.48 | 0.46 | 0.47 | 0.46 | 0.47 | 0.47 | 0.67 | 0.66 | 0.66 | 0.66 | 0.66 | 0.68 | 0.67 | 0.67 | 0.67 | 0.67 |
| 0.28 | 0.52 | 0.55 | 0.52 | 0.52 | 0.53 | 0.51 | 0.51 | 0.50 | 0.50 | 0.51 | 0.50 | 0.50 | 0.50 | 0.50 | 0.51 | 0.49 | 0.52 | 0.51 | 0.50 | 0.52 |
| 3.20 | 2.33 | 2.35 | 2.34 | 2.34 | 2.35 | 2.45 | 2.46 | 2.46 | 2.44 | 2.46 | 3.04 | 3.06 | 3.04 | 3.06 | 3.06 | 3.06 | 3.10 | 3.11 | 3.08 | 3.07 |
| 2.42 | 0.92 | 0.94 | 0.94 | 0.92 | 0.92 | 1.02 | 1.01 | 1.00 | 1.02 | 1.02 | 2.11 | 2.06 | 2.05 | 2.06 | 2.09 | 2.34 | 2.36 | 2.35 | 2.34 | 2.37 |
| <0.01 | <0.01 | <0.01 | <0.01 | <0.01 | <0.01 | <0.01 | <0.01 | <0.01 | <0.01 | <0.01 | <0.01 | <0.01 | <0.01 | <0.01 | <0.01 | <0.01 | <0.01 | <0.01 | <0.01 | <0.01 |
| 26.37 | 28.59 | 28.41 | 28.32 | 28.59 | 28.37 | 28.33 | 28.58 | 28.74 | 28.47 | 28.57 | 27.10 | 27.04 | 27.26 | 27.29 | 27.26 | 26.78 | 26.87 | 26.85 | 26.91 | 26.82 |
| 2.53 | 3.01 | 3.06 | 3.06 | 3.05 | 3.06 | 3.05 | 3.07 | 3.03 | 3.09 | 3.10 | 2.57 | 2.55 | 2.63 | 2.62 | 2.60 | 2.83 | 2.85 | 2.83 | 2.79 | 2.82 |
| 1.48 | 1.91 | 1.90 | 1.92 | 1.90 | 1.91 | 1.76 | 1.79 | 1.77 | 1.78 | 1.78 | 1.35 | 1.34 | 1.32 | 1.33 | 1.35 | 1.08 | 1.09 | 1.07 | 1.05 | 1.05 |
| 14.76 | 11.31 | 11.24 | 11.28 | 11.23 | 11.20 | 11.12 | 11.12 | 11.07 | 11.11 | 11.11 | 13.79 | 13.58 | 13.63 | 13.65 | 13.72 | 13.77 | 13.82 | 13.84 | 13.83 | 13.79 |
| 0.31 | 0.59 | 0.62 | 0.59 | 0.59 | 0.60 | 0.58 | 0.58 | 0.57 | 0.57 | 0.58 | 0.56 | 0.57 | 0.57 | 0.57 | 0.58 | 0.56 | 0.60 | 0.57 | 0.57 | 0.59 |
| 10.74 | 8.76 | 8.78 | 8.72 | 8.77 | 8.71 | 8.81 | 8.82 | 8.72 | 8.83 | 8.85 | 10.79 | 10.83 | 10.82 | 10.92 | 10.83 | 8.44 | 8.47 | 8.43 | 8.45 | 8.47 |
| 20.86 | 22.44 | 22.51 | 22.44 | 22.42 | 22.47 | 22.54 | 22.67 | 22.56 | 22.60 | 22.57 | 22.18 | 22.26 | 22.20 | 22.22 | 22.25 | 20.35 | 20.37 | 20.35 | 20.26 | 20.34 |
| 10.19 | 12.08 | 12.14 | 12.15 | 12.09 | 12.09 | 12.13 | 12.30 | 12.16 | 12.22 | 12.32 | 9.95 | 9.92 | 9.90 | 10.02 | 9.93 | 12.21 | 12.09 | 12.10 | 12.11 | 12.09 |
| <0.01 | <0.01 | <0.01 | <0.01 | <0.01 | <0.01 | <0.01 | <0.01 | <0.01 | <0.01 | <0.01 | <0.01 | <0.01 | <0.01 | <0.01 | <0.01 | <0.01 | <0.01 | <0.01 | <0.01 | <0.01 |
| <0.01 | <0.01 | <0.01 | <0.01 | <0.01 | <0.01 | <0.01 | <0.01 | <0.01 | <0.01 | <0.01 | <0.01 | <0.01 | <0.01 | <0.01 | <0.01 | <0.01 | <0.01 | <0.01 | <0.01 | <0.01 |
| 2.30 | 3.58 | 3.55 | 3.57 | 3.55 | 3.58 | 3.41 | 3.48 | 3.51 | 3.42 | 3.47 | 2.37 | 2.38 | 2.38 | 2.46 | 2.40 | 4.05 | 4.09 | 4.09 | 4.09 | 4.16 |
| 0.04 | 0.03 | 0.02 | 0.10 | 0.05 | 0.03 | 0.06 | 0.05 | 0.02 | 0.03 | 0.03 | <0.01 | 0.06 | 0.07 | 0.09 | 0.06 | 0.02 | 0.05 | <0.01 | <0.01 | 0.03 |
| 2.01 | 2.09 | 2.02 | 2.11 | 2.07 | 2.00 | 2.07 | 2.06 | 2.09 | 1.99 | 2.10 | 2.08 | 2.19 | 2.03 | 2.04 | 2.01 | 2.72 | 2.68 | 2.81 | 2.79 | 2.75 |
| 0.88 | 0.81 | 0.84 | 0.78 | 0.80 | 0.81 | 0.79 | 0.82 | 0.83 | 0.85 | 0.86 | 0.87 | 0.88 | 0.89 | 0.85 | 0.95 | 1.11 | 1.12 | 1.13 | 1.10 | 1.18 |
| 0.23 | 0.16 | 0.14 | 0.15 | 0.19 | 0.18 | 0.20 | 0.17 | 0.18 | 0.17 | 0.17 | 0.23 | 0.20 | 0.23 | 0.18 | 0.19 | 0.23 | 0.23 | 0.24 | 0.20 | 0.24 |
| 0.13 | 0.07 | 0.07 | 0.08 | 0.07 | 0.07 | 0.07 | 0.09 | 0.05 | 0.07 | 0.06 | <0.02 | <0.02 | <0.02 | <0.02 | <0.02 | <0.02 | <0.02 | <0.02 | <0.02 | <0.02 |
| 0.73 | 0.52 | 0.50 | 0.52 | 0.51 | 0.52 | 0.49 | 0.51 | 0.50 | 0.51 | 0.51 | 0.72 | 0.71 | 0.71 | 0.71 | 0.71 | 0.73 | 0.72 | 0.72 | 0.73 | 0.72 |
| 99.16 | 99.18 | 99.08 | 99.06 | 99.14 | 98.87 | 98.88 | 99.54 | 99.26 | 99.18 | 99.55 | 99.72 | 99.60 | 99.72 | 100.07 | 99.99 | 100.27 | 100.49 | 100.50 | 100.29 | 100.50 |
| Based on 4 oxygens | | | | | | | | | | | | | | | | | | | | |
| 0.31 | 0.33 | 0.33 | 0.33 | 0.33 | 0.33 | 0.33 | 0.33 | 0.33 | 0.33 | 0.33 | 0.33 | 0.33 | 0.33 | 0.32 | 0.33 | 0.30 | 0.30 | 0.30 | 0.30 | 0.30 |
| 0.15 | 0.17 | 0.17 | 0.17 | 0.17 | 0.17 | 0.17 | 0.17 | 0.17 | 0.17 | 0.17 | 0.14 | 0.14 | 0.14 | 0.14 | 0.14 | 0.17 | 0.17 | 0.17 | 0.17 | 0.17 |
| 0.16 | 0.13 | 0.13 | 0.13 | 0.13 | 0.13 | 0.13 | 0.13 | 0.13 | 0.13 | 0.13 | 0.16 | 0.16 | 0.16 | 0.16 | 0.16 | 0.12 | 0.12 | 0.12 | 0.12 | 0.13 |
| 0.07 | 0.05 | 0.05 | 0.05 | 0.05 | 0.05 | 0.05 | 0.05 | 0.05 | 0.05 | 0.05 | 0.06 | 0.07 | 0.06 | 0.06 | 0.06 | 0.07 | 0.07 | 0.07 | 0.07 | 0.07 |
| 0.14 | 0.10 | 0.10 | 0.10 | 0.10 | 0.10 | 0.10 | 0.10 | 0.10 | 0.10 | 0.10 | 0.13 | 0.12 | 0.12 | 0.12 | 0.12 | 0.13 | 0.13 | 0.13 | 0.13 | 0.13 |
| 0.00 | 0.01 | 0.01 | 0.01 | 0.01 | 0.01 | 0.01 | 0.01 | 0.01 | 0.01 | 0.01 | 0.01 | 0.01 | 0.01 | 0.01 | 0.01 | 0.00 | 0.01 | 0.01 | 0.01 | 0.01 |
| 0.00 | 0.00 | 0.00 | 0.00 | 0.00 | 0.00 | 0.00 | 0.00 | 0.00 | 0.00 | 0.00 | 0.00 | 0.00 | 0.00 | 0.00 | 0.00 | 0.00 | 0.00 | 0.00 | 0.00 | 0.00 |
| 0.06 | 0.08 | 0.08 | 0.08 | 0.08 | 0.08 | 0.08 | 0.08 | 0.08 | 0.08 | 0.08 | 0.06 | 0.06 | 0.06 | 0.06 | 0.06 | 0.05 | 0.05 | 0.05 | 0.05 | 0.05 |
| 0.00 | 0.00 | 0.00 | 0.00 | 0.00 | 0.00 | 0.00 | 0.00 | 0.00 | 0.00 | 0.00 | 0.00 | 0.00 | 0.00 | 0.00 | 0.00 | 0.00 | 0.00 | 0.00 | 0.00 | 0.00 |
| 0.01 | 0.01 | 0.01 | 0.01 | 0.01 | 0.01 | 0.01 | 0.01 | 0.01 | 0.01 | 0.01 | 0.01 | 0.01 | 0.01 | 0.01 | 0.01 | 0.01 | 0.01 | 0.01 | 0.01 | 0.01 |
| 0.04 | 0.04 | 0.04 | 0.04 | 0.04 | 0.04 | 0.04 | 0.04 | 0.04 | 0.04 | 0.04 | 0.04 | 0.04 | 0.04 | 0.04 | 0.04 | 0.04 | 0.04 | 0.04 | 0.04 | 0.04 |
| 0.03 | 0.05 | 0.05 | 0.05 | 0.05 | 0.05 | 0.05 | 0.05 | 0.05 | 0.05 | 0.05 | 0.03 | 0.03 | 0.03 | 0.03 | 0.03 | 0.06 | 0.06 | 0.06 | 0.06 | 0.06 |
| 0.00 | 0.00 | 0.00 | 0.00 | 0.00 | 0.00 | 0.00 | 0.00 | 0.00 | 0.00 | 0.00 | 0.00 | 0.00 | 0.00 | 0.00 | 0.00 | 0.00 | 0.00 | 0.00 | 0.00 | 0.00 |
| 0.03 | 0.03 | 0.03 | 0.03 | 0.03 | 0.03 | 0.03 | 0.03 | 0.03 | 0.03 | 0.03 | 0.03 | 0.03 | 0.03 | 0.03 | 0.03 | 0.04 | 0.04 | 0.04 | 0.04 | 0.04 |
| 0.01 | 0.01 | 0.01 | 0.01 | 0.01 | 0.01 | 0.01 | 0.01 | 0.01 | 0.01 | 0.01 | 0.01 | 0.01 | 0.01 | 0.01 | 0.01 | 0.01 | 0.01 | 0.01 | 0.01 | 0.02 |
| 0.00 | 0.00 | 0.00 | 0.00 | 0.00 | 0.00 | 0.00 | 0.00 | 0.00 | 0.00 | 0.00 | 0.00 | 0.00 | 0.00 | 0.00 | 0.00 | 0.00 | 0.00 | 0.00 | 0.00 | 0.00 |
| 1.00 | 1.00 | 1.01 | 1.01 | 1.00 | 1.01 | 1.00 | 1.00 | 1.00 | 1.00 | 1.00 | 1.00 | 1.00 | 1.00 | 1.00 | 1.00 | 1.00 | 1.00 | 1.00 | 1.00 | 1.00 |
| 0.90 | 0.96 | 0.96 | 0.96 | 0.96 | 0.96 | 0.96 | 0.96 | 0.96 | 0.96 | 0.96 | 0.92 | 0.92 | 0.92 | 0.92 | 0.92 | 0.91 | 0.91 | 0.91 | 0.91 | 0.91 |
| 0.10 | 0.04 | 0.04 | 0.04 | 0.04 | 0.04 | 0.04 | 0.04 | 0.04 | 0.04 | 0.04 | 0.08 | 0.08 | 0.08 | 0.08 | 0.08 | 0.09 | 0.09 | 0.09 | 0.09 | 0.09 |
| 0.00 | 0.00 | 0.00 | 0.00 | 0.00 | 0.00 | 0.00 | 0.00 | 0.00 | 0.00 | 0.00 | 0.00 | 0.00 | 0.00 | 0.00 | 0.00 | 0.00 | 0.00 | 0.00 | 0.00 | 0.00 |
| 0.00 | 0.00 | 0.00 | 0.00 | 0.00 | 0.00 | 0.00 | 0.00 | 0.00 | 0.00 | 0.00 | 0.00 | 0.00 | 0.00 | 0.00 | 0.00 | 0.00 | 0.00 | 0.00 | 0.00 | 0.00 |
| 1.00 | 1.00 | 1.00 | 1.00 | 1.00 | 1.00 | 1.00 | 1.00 | 1.01 | 1.00 | 1.00 | 1.00 | 1.00 | 1.01 | 1.00 | 1.00 | 1.00 | 1.00 | 1.00 | 1.01 | 1.00 |

et al., 1984) suggest that the entire Bamble lithotectonic unit is dominated by Group 1 pegmatites (Fig. 2). There are no coeval granite intrusions exposed in the entire unit. The only granite intrusion exposed are the Herefoss and Grimstad granites, which are at least ~ 130 Ma (Andersen, 1997) and 70 Ma (Kullerud and Machado, 1991), respectively, younger than the pegmatites. According to the regional Bouguer anomaly field (Gellein, 2003, 2007), the area is dominated by high-density rocks with no indications of a granite pluton below the surface up to 10 km depth. The lack of granites suggest that another process is responsible for the genesis of these pegmatites. The pegmatites of the Bamble lithotectonic unit postdate the peak of the amphibolite- to granulite-facies metamorphism, which is recorded between 1147 ± 12 and 1122 ± 8 Ma (Bingen et al., 2008b, 2021; Bingen and Viola, 2018; Engvik et al., 2016; Nijland et al., 2014). The Group 1 pegmatite ages overlap with titanite and monazite U-Pb data of gneisses raning from 1107 ± 9 to 1091 ± 2 Ma (Bingen et al., 2008b; Cosca et al., 1998; deHaas et al., 2002) and amphibole Ar-Ar plateau ages ranging from 1099 ± 3 to 1079 ± 5 Ma and with the timing of widespread metasomatism as recorded by rutile data (Engvik et al., 2011, 2018). These younger ages seem to be related to the thrusting of the Bamble unit onto the Telemark lithotectonic unit and, thus, may be related to post-peak transpression.

The thickening was accompanied by transpressional shearing which resulted in several km long, NE-SW striking fault zones (e.g., Starmer, 1993; Fig. 2), which are dated to around 1060 Ma (Field and Råheim, 1981). Hutton and Reavy (1992) and Druguet and Hutton (1998) describe anatectic pegmatites that formed in a transpressional regime related with ductile shear zones from Iberia and the eastern Pyrenees. They argue that the tectonic process is the local trigger for melt generation and that shear zones control the ascent path and emplacement of the melts that eventually formed the pegmatites. Henderson and Ihlen (2004) and Müller et al. (2015) proposed a similar process for the formation of the pegmatites of the Froland field at the western margin of the Bamble lithotectonic unit. Thus, melting along shear zones also may have formed the Kragerø pegmatites. Transpressional thickening of the crust and related shearing potentially triggered melting that led to the

**Table 4**
Average monazite ages.

| Pegmatite | Field | Method | Average age | Uncertainty | No. * |
|---|---|---|---|---|---|
| Herrebøkasa | Østfold | U-Th-Pb EPMA | 903.2 | 9.5 | 7 |
| Bjønnetjønn | Østfold | U-Th-Pb EPMA | 984 | 12 | 5 |
| Bjertnes | Flesberg | U-Th-Pb EPMA | 908 | 12 | 4 |
| Hullerøya 2 | Kragerø | U-Th-Pb EPMA | 1067 | 10 | 5 |
| Bråten 2 | Kragerø | U-Th-Pb EPMA | 1057 | 10 | 5 |
| Bjønndalen | Kragerø | U-Th-Pb EPMA | 1064 | 10 | 5 |
| Upper Høydalen | Tørdal | U-Pb ID-TIMS | 905.0 | 2.4 | 3 |

* Number of analyses included in the age calculation.

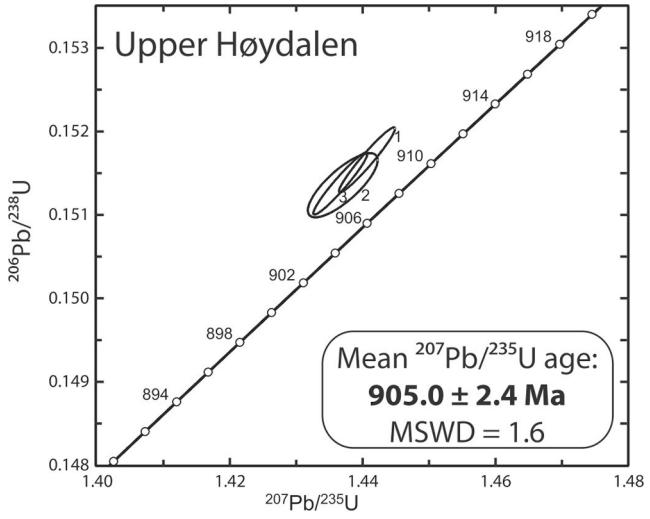


**Fig. 8.** Concordia diagram showing U-Pb ID-TIMS data for monazite from the Upper Høydalen pegmatite (Tørdal). Note, the measured ratios fall above the concordia curve because of excess $^{206}$Pb, which is derived from $^{230}$Th (Schärer, 1984). Excess $^{206}$Pb does not affect the $^{207}$Pb /$^{235}$U age and, therefore, the weighted $^{207}$Pb /$^{235}$U ratios yield the best age estimate. The small numbers correspond to analysis numbers in Table 5.

formation of the Kragerø pegmatites. In addition, the rocks of the Bamble lithotectonic unit underwent extensive metasomatism coeval with the pegmatite formation (Engvik et al., 2011, 2018). The metasomatic fluids possibly lowered the melting temperature of the rocks and thereby contributed to the formation of the pegmatite melts.

Group 1 pegmatites in the *Idefjorden lithotectonic unit* range in age from 1041 to 1030 Ma (Romer and Smeds, 1996; Müller et al., 2017; Narum et al., 2022) and are younger than Group 1 pegmatites from the Bamble lithotectonic unit. The new age for the Spro pegmatite of 1035 ± 2 Ma coincides with the other Group 1 pegmatites in the Idefjorden lithotectonic unit (Fig. 5) and is also similar to the zircon age of 1051 ± 5 Ma reported for another pegmatite (Agnor) of the area by Bue (2005), although the latter age may somewhat be too old due to inheritance. The pegmatite formation overlaps with high-grade metamorphism in the Idefjorden lithotectonic unit at 1050 to 1025 Ma (Söderlund et al., 2008). There are, however, no granites coeval to Group 1 pegmatites exposed. The high-grade metamorphism probably led to local anatexis related to shear zones, forming pegmatite melts as suggested by Müller et al. (2017). The pegmatites align N—S to NW-SE parallel to major shear zones. The alignment and proximity to the shear zones indicate a tectonic control on crustal melting (Müller et al., 2017). Thus, Group 1 pegmatites in the Idefjorden and Bamble lithotectonic units formed in a similar way.

### 5.1.2. *Tectonic setting of Group 2 pegmatites (930–890 Ma)*

The new age of the Upper Høydalen pegmatite (905.0 ± 2.4 Ma) and Skardsfjell (892.7 ± 8.8 Ma) are the first age data from the Tørdal pegmatite field in the central-south Telemark lithotectonic unit. The Tørdal pegmatite field occurs northeast of the Tørdal-Treungen granite which has been inferred to be the source of the pegmatite melts (Bergstøl and Juve, 1988). The age of the Tørdal-Treungen granite itself requires discussion. The Tørdal-Treungen granite is a large (c. 40 × 15 km) pluton is characterized by high concentration in radioelements. A granite pluton of that size may take several million years to crystallize (Paterson and Tobisch, 1992). Also, the pluton is possibly a composite batholith. The age of 918 ± 7 Ma (Andersen et al., 2007a) is based on one concordant ICP-MS analysis from a larger set of highly discordant analyses reflecting both inheritance and metamictization of unusually U-rich (up to 6000 ppm) zircon. This age estimate is not robust. The U-Pb zircon age of 957 ± 12 Ma (Slagstad et al., 2018) is collected from a sample in the western and central part of the Tørdal-Treungen granite, and may represent an early phase of the plutonic complex. Our new zircon and Nb-Y-oxide age of 946 ± 4 Ma is overlapping with the published age of 957 ± 12 Ma. It is representative of the northeastern part of the pluton and is the most relevant for discussing the relation between the pluton and the pegmatites. Collectively, the data indicate that the pegmatites (905.0 ± 2.4 Ma and 892.7 ± 8.8 Ma) formed approximately 40 m.y. after the emplacement of the granite pluton (946 ± 4 Ma). The time gap between granite and pegmatite crystallization is too large to interpret the pegmatite melts as late evolved pluton-derived melts, even if the Tørdal-Treungen granite is interpreted as a polyphase pluton. The regional Bouguer anomaly field does not favour the existence of a hidden younger granite (Gellein, 2007). Thus, the Tørdal-Treungen granite is unlikely to be the source of the Tørdal pegmatites. Similar to other Group 1 pegmatite fields, the Tørdal pegmatites are hosted by amphibolites. Various lines of evidence for partial melting are present in outcrops. For example, in the Kleppe quarry in the centre of the pegmatite field, many hair-fine leucosome veins in amphibolite unite to and develop over a distance of a few meters into meter-wide pegmatite veins, indicating that partial melting of amphibolite may form pegmatite melts (Fig. 3 in Steffenssen et al., 2020). Similar partial melting textures in amphibolite are exposed at the "Iveland wall" in the centre of the Evje-Iveland pegmatite field (Fig. 12 in Müller et al., 2017). The Evje-Iveland pegmatites formed by partial melting of their amphibolite country rocks (Müller et al., 2015, 2017; Snook, 2014). Based on the discordant regional chemical zoning (with respect to the Tørdal granite contact), the age gap and the evidence for *in situ* melting of amphibolite host rocks we suggest that the Tørdal pegmatites, like the Evje-Iveland pegmatites, formed by direct anatectic melting of their host rock.

The Bjertnes pegmatite from the Flesberg pegmatite field in the northeast of the Telemark lithotectonic unit has a similar crystallization age (908 ± 12 Ma) as other Group 2 pegmatites in the Telemark unit (Tørdal and Evje-Iveland fields). The field occurs in an area with no exposed granite intrusion (Fig. 4). The Bjertnes pegmatite is hosted in the Hallingdal complex comprising quartzite, granitic gneiss and minor amphibolite. A granitic gneiss collected near the pegmatite yields an age of 1499 ± 10 Ma (sample B99120 of Bingen and Viola, 2018). Similar chemistry, timing and the absence of a potential parental granite suggest that the Flesberg pegmatites formed in the same way as the other Telemark-unit-hosted Group 2 pegmatites.

In the Bamble lithotectonic unit, Group 2 pegmatites occur exclusively at the southernmost tip of the unit comprising the Kristiansand pegmatite field. In fact, most of the Kristiansand pegmatites occur in a cluster spreading on both sides of the Porsgrunn-Kristiansand fault zone, which separates the Bamble from the Telemark lithotectonic unit (Fig. 2). Some of the Kristiansand pegmatites occur in the Telemark lithotectonic unit. In this part of the Bamble lithotectonic unit, the fault

**Table 5**
U-Pb ID-TIMS monazite, zircon and Nb-Y-oxide age data.

| Sample | Weight (μg) | Concentrations (ppm) | | $^{206}Pb/^{204}Pb$ | Common lead (pg) | Th/U | Atomic ratios | | | | | | Apparent ages (Ma) | | |
|---|---|---|---|---|---|---|---|---|---|---|---|---|---|---|---|
| | | U | Pb (tot) | Measured ratios | Pb(tot)-Pb(rad) | | $^{206}Pb/^{238}U$ | 2σ (abs) | $^{207}Pb/^{235}U$ | 2σ (abs) | $^{207}Pb/^{206}Pb$ | 2σ (abs) | $^{206}Pb/^{238}U$ | $^{207}Pb/^{235}U$ | $^{207}Pb/^{206}Pb$ |
| (a) | | | | (b) | (c) | (d) | (e) | | (e) | | (e) | | (e) | (e) | (e) |
| **Tørdal granite** | | | | | | | | | | | | | | | |
| Zircon-1 | ≤1 | >1445 | >219 | 13,371 | 1.0 | 0.27 | 0.15288 | 0.00044 | 1.5373 | 0.0050 | 0.07293 | 0.00008 | 917.1 | 945.4 | 1011.9 |
| Zircon-2 | ≤1 | >1808 | >270 | 1786 | 8.8 | 0.48 | 0.14151 | 0.00034 | 1.3575 | 0.0041 | 0.06957 | 0.00010 | 853.2 | 870.8 | 915.8 |
| Zircon-3 | ≤1 | >1658 | >236 | 9331 | 1.5 | 0.55 | 0.13494 | 0.00035 | 1.2876 | 0.0039 | 0.06921 | 0.00007 | 816.0 | 840.2 | 904.9 |
| Zircon-4 | ≤1 | >2413 | >365 | 1249 | 17 | 0.36 | 0.14463 | 0.00041 | 1.3858 | 0.0048 | 0.06949 | 0.00012 | 870.8 | 882.9 | 913.4 |
| Zircon-5 | ≤1 | >849 | >93 | 1342 | 4.2 | 0.46 | 0.10688 | 0.00026 | 0.9689 | 0.0034 | 0.06574 | 0.00015 | 654.6 | 687.9 | 798.2 |
| Zircon-6 | ≤1 | >3094 | >316 | 4791 | 4.0 | 0.46 | 0.10009 | 0.00031 | 0.8917 | 0.0030 | 0.06462 | 0.00006 | 614.9 | 647.3 | 761.9 |
| Nb-Y-oxide-1 | ≤1 | >48114 | >7906 | 6119 | 73 | 0.57 | 0.15204 | 0.00035 | 1.4713 | 0.0039 | 0.07018 | 0.00006 | 912.4 | 918.7 | 933.7 |
| Nb-Y-oxide-2 | ≤1 | >67607 | >10772 | 3891 | 158 | 0.54 | 0.14805 | 0.00037 | 1.4282 | 0.0042 | 0.06996 | 0.00007 | 890.0 | 900.8 | 927.3 |
| Nb-Y-oxide-3 | ≤1 | >73479 | >11213 | 3417 | 185 | 0.60 | 0.14012 | 0.00039 | 1.3392 | 0.0043 | 0.06932 | 0.00008 | 845.3 | 862.9 | 908.1 |
| Nb-Y-oxide-4 | ≤1 | >170010 | >26133 | 1991 | 746 | 0.52 | 0.14187 | 0.00055 | 1.3622 | 0.0090 | 0.06964 | 0.00012 | 855.2 | 872.8 | 917.7 |
| Nb-Y-oxide-5 | ≤1 | >50216 | >7865 | 11,890 | 37.7 | 0.58 | 0.14594 | 0.00045 | 1.4129 | 0.0049 | 0.07022 | 0.00007 | 878.2 | 894.4 | 934.7 |
| Th-U-oxide-1 | ≤1 | >229500 | >15512 | 13,624 | 44.4 | 3.25 | 0.04306 | 0.00021 | 0.3307 | 0.0017 | 0.05570 | 0.00005 | 271.8 | 290.1 | 440.4 |
| **Upper Høydalen pegmatite** | | | | | | | | | | | | | | | |
| Monazite-1 | 20 | 577 | 650 | 20,126 | 5.5 | 23.90 | 0.15166 | 0.00032 | 1.4407 | 0.00 | 0.06890 | 0.00005 | 910.3 | 906.0 | 895.6 |
| Monazite-2 | 26 | 38 | 48 | 2596 | 3.6 | 27.13 | 0.15135 | 0.00031 | 1.4370 | 0.00 | 0.06886 | 0.00013 | 908.5 | 904.5 | 894.5 |
| Monazite-3 | 34 | 341 | 400 | 16,357 | 6.7 | 25.05 | 0.15138 | 0.00030 | 1.4367 | 0.00 | 0.06883 | 0.00005 | 908.7 | 904.3 | 893.7 |

(a) single grain analyses.- Ziircon grains air abraded before dissolution, oxides and monazite not abraded.
(b) raw data corrected for fractionation and blank.
(c) Pbc = total common Pb in sample (initial + blank).
(d) Th/U model ratio inferred from 208/206 ratio and age of sample.
(e) corrected for fractionation, spike, blank and initial common Pb; error calculated by propagating the main sources of uncertainty;

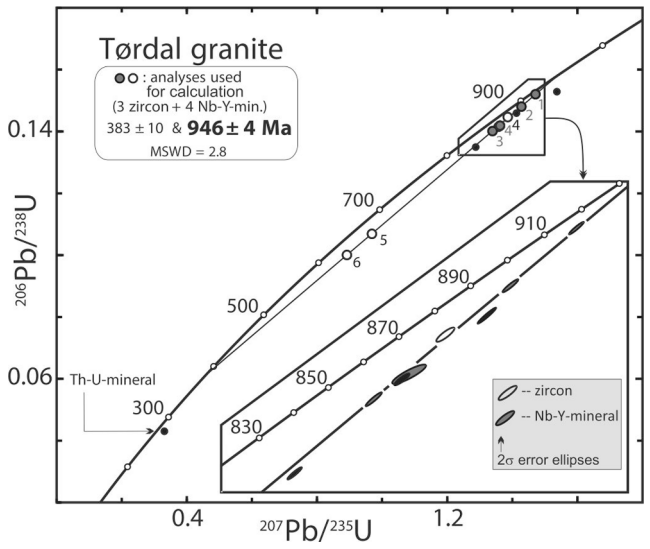


**Fig. 9.** Concordia diagram showing U-Pb ID-TIMS data for zircon and Nb-Y-oxide from the Tørdal granite. The small numbers correspond to analysis numbers in Table 5.

zone separating it from the Telemark lithotectonic unit is less clearly defined than further to the northeast. Rocks on both sides of the fault zone are similar suggesting only minor displacements. The Kristiansand pegmatites and the Evje-Iveland and Tørdal pegmatites fall in the same age group and all are mainly hosted by amphibolites. Thus, the Kristiansand pegmatites and the Tørdal and Evje-Iveland pegmatites may have formed in a similar tectonic setting and by similar processes, i.e. partial melting of the host rock.

The setting of the Group 2 pegmatites of the Idefjorden lithotectonic unit, i.e. the Østfold pegmatite field, differs from the other Group 2 pegmatites in two respects: First, these pegmatites overlap in age with their adjacent granites, the Iddefjord and Bohus plutons, and, second, they occur together with Group 1 pegmatites in the same field (Fig. 1). The age overlap of pegmatites and granites implies that Group 2 pegmatites of the Østfold pegmatite field may have a different melting history than other Group 2 pegmatites. Müller et al. (2017) proposed that the pegmatite melts might represent fractionated, residual melts of the granite intrusions. However, there are several observations, which do not fit to classical setting of pluton-derived pegmatites. First, there is no chemical zonation in the Østfold pegmatite field, as would be expected if the pegmatites are related to a central granite (e.g., Černy, 1991b). The close relation between granite and pegmatite field may be indirect with the emplacement of the granite pluton providing the heat for partial melting of the intruded paragneisses. Such a scenario was discussed by Fuchsloch et al. (2018) for the post-tectonic granites and pegmatites in the Damara Orogen (Namibia). If the granite source provides the heat source for melting of the paragneisses, there is a temporal relation, but there should be no chemical zonation within Østfold pegmatite field relative to the Iddefjord granite.

### 5.2. Pegmatite formation stages and their relation to the Sveconorwegian orogeny

The two periods of widespread pegmatite formation correspond to two high-temperature events of the Sveconorwegian orogeny. Group 1 pegmatites in the Bamble and Kongsberg lithotectonic units postdate amphibolite- to granulite-facies peak metamorphism in the area and are coeval with widespread Na-metasomatism (scapolitization and albitization) and associated with younger (1110 to 1080 Ma), retrograde amphibolite-facies metamorphism with temperatures of 600 to 700 °C and 2–4 kbar at 1104 ± 7 Ma (e.g., Lieftink et al., 1994; Nijland and Touret, 2001; Engvik et al., 2009, 2011) and with shearing related to the NW-directed thrusting of the Bamble lithotectonic unit onto the Telemark lithotectonic unit (Henderson and Ihlen, 2004). This shearing has not been dated directly, but Group 1 pegmatites are kinematically related to overthrust geometries associated with the initial thrusting phase of the Porsgrunn-Kristiansand fault zone when the Bamble unit docked with the underlying Telemark unit (Henderson and Ihlen, 2004). In the Idefjorden lithotectonic unit, Group 1 pegmatites are coeval with high-grade metamorphism (1043 ± 11 Ma and 1024 ± 9 Ma; Åhäll et al., 1998; Austin Hegardt 2010; Austin Hegardt et al. 2007; Bingen et al. 2008a), regional migmatitisation (1039 ± 17 to 997 ± 16 Ma, Bingen et al., 2021) and related to NW-SE directed shearing (Viola et al., 2011). Group 2 pegmatites formed in an extensional regime predominantly affecting the Telemark and Idefjorden lithotectonic units during the late stages of the Sveconorwegian orogeny and overlap in age with the emplacement of the anorthosite-mangerite-charnockite suite of the Rogaland Igneous Complex (937 ± 1 and 916 ± 9 Ma; Bolle et al., 2018; Schärer et al., 1996; Vander Auwera et al., 2011; 2014) at the SW edge of the Telemark lithotectonic unit. During these late stages of the Sveconorwegian orogeny, the continental crust experienced a high thermal gradient due to crustal thinning and accompanied underplating by mafic magma (Vander Auwera et al., 2003, 2014; Andersen et al., 2007b; Slagstad et al., 2018; Granseth et al., 2020). The underplating magma provided the heat source for crustal melting leading to the formation of the hornblende-biotite granite suite at 1000–920 Ma (e.g. Andersen et al., 2002, Granseth et al., 2020) and Group 2 pegmatites.

Mafic underplating is known to occur in pulses by periodic influx of basaltic magma into the lower crust (e.g. Petford and Gallagher, 2001). The Rogaland Igneous Complex, emplaced at the SW edge of the Telemark lithotectonic unit at 937–916 Ma, is the surface expression of such mafic magma underplating (Andersen et al., 2007b; Bolle et al., 2018; Bybee et al., 2014; Schärer et al., 1996). The regional distribution of Group 2 pegmatites suggests that partial melting caused by mafic underplating seems to be restricted to parts of the Telemark and Idefjorden units (see Andersen et al., 2007b). Group 2 pegmatites are irregularly spread in the Telemark lithotectonic unit and seem to be controlled by the type of host rock. Group 2 pegmatites occur mainly in areas dominated by amphibolites and amphibole gneisses and to a much lesser extent in the surrounding granitic basement gneisses. This applies also to the majority of Group 1 pegmatites which are hosted by amphibole-biotite gneisses often close to or at the contact to amphibolite bodies. This observation implies that amphibolites are more fertile for NYF-type pegmatite formation than the granitic gneisses. In contrast, in the Østfold lithotectonic unit Group 2 pegmatites formed coevally with hornblende-biotite granites and in the same area.

### 5.3. Possible sources of NYF pegmatite melts

The two identified Sveconorwegian pegmatite forming events produced a high quantity of large (>1000 $m^3$) pegmatites with NYF affinity together with pegmatites representing different chemical–mineralogical transitions from NYF pegmatites to simple abyssal pegmatites (Müller et al., 2017). The majority of Group 1 and Group 2 pegmatites are hosted by rocks of intermediate to mafic compositions: granodioritic, biotite- and biotite-amphibole gneisses and amphibolites. The consistent chemical NYF affinity of the pegmatites suggests that the melts are derived either from mafic rocks or A-type granites (biotite- and biotite-amphibole gneisses) (e.g. Černý, 1991a; Martin et al., 2008). So far, no Sveconorwegian LCT pegmatites, which are derived from metasedimentary or S-type granitic rocks, have been described form southern Scandinavia.

Beside the different formation periods and occurrence in different lithotectonic units, three additional major differences exist in the chemistry and location of Group 1 and Group 2 pegmatites. First, the chemical NYF - affinity (higher abundances of REE and F) is generally stronger in Group 2 than in Group 1 pegmatites (Table 7). Second, Group 2 pegmatites are predominantly hosted in amphibole gneisses and

**Table 6**
Age relations of pegmatites and neighbouring granites. The minimum age difference refers to pegmatites and neighbouring granites.

| Pegmatite field | Litho-tectonic unit | Pegmatite | Pegmatite age (Ma) | Neighboring granite | Age of neighboring granite (Ma) | Minimum age difference (Ma) | Pegmatite group |
|---|---|---|---|---|---|---|---|
| Göteborg | Idefjorden | Högsbo | 1029.7 ± 1.4 (Romer and Smeds 1996) | No granite exposed | – | – | 1 |
| Østfold | Idefjorden | Spro | 1035.5 ± 2.2* | No granite exposed | – | – | 1 |
| Østfold | Idefjorden | Agnor | 1051 ± 5 (Bue 2005) | No granite exposed | – | – | 1 |
| Østfold | Idefjorden | Remmen | 1041–1033 (Narum et al. 2022) | Bohus | 922 ± 5 (Eliasson and Schöberg 1991) | 106 | 1 |
| Halland | Idefjorden | Timmerhult | 1038.7 ± 3.4 (Romer and Smeds 1996) | Bohus | 922 ± 5 (Eliasson and Schöberg 1991) | 108 | 1 |
| Halland | Idefjorden | Skantorp | 1041.3 ± 1.6 (Romer and Smeds 1996) | Bohus | 922 ± 5 (Eliasson and Schöberg 1991) | 113 | 1 |
| Froland | Bamble | Gloserheia | 1060 + 8/-6 (Baadsgaard et al. 1984) | Holtebu, Herefoss | 926 ± 8 (Andersen 1997) | 122 | 1 |
| Kragerø | Bamble | Tangen | 1082.2 ± 4.8* | No granite exposed | – | – | 1 |
| Kragerø | Bamble | Tangen | 1082.3 ± 4.5 (Müller et al. 2017) | No granite exposed | – | – | 1 |
| Kragerø | Bamble | Bråten 2 | 1057 ± 10* | No granite exposed | | – | 1 |
| Kragerø | Bamble | Bjønndalen | 1064 ± 10* | No granite exposed | | – | 1 |
| Kragerø | Bamble | Hullerøya 2 | 1067 ± 10* | No granite exposed | | – | 1 |
| Arendal | Bamble | Tvedestrand | 1094 ± 11 (Scherer et al. 2001) | No granite exposed | – | – | 1 |
| Tørdal | Telemark | Skardsfjell | 892.7 ± 8.8* | Tørdal | 946 ± 4* | 41 | 2 |
| Tørdal | Telemark | Upper Høydalen | 905.0 ± 2.4* | Tørdal | 946 ± 4* | 35 | 2 |
| Evje-Iveland | Telemark | Mølland | 900.7 ± 1.8 (Müller et al. 2017) | Høvringsvatnet | 981 ± 6 (Snook 2014) | 63 | 2 |
| Evje-Iveland | Telemark | Mølland | 906 ± 9 (Seydoux-Guillaume et al. 2012) | Høvringsvatnet | 981 ± 6 (Snook 2014) | 64 | 2 |
| Evje-Iveland | Telemark | Frikstad | 910 ± 14 (Scherer et al. 2001) | Høvringsvatnet | 981 ± 6 (Snook 2014) | 61 | 2 |
| Evje-Iveland | Telemark | Steli | 910.2 ± 7.1 (Müller et al. 2017) | Høvringsvatnet | 981 ± 6 (Snook 2014) | 52 | 2 |
| Hidra | Telemark | Hidra | 911 ± 3 (Müller et al. 2017) | No granite exposed | – | – | 2 |
| Farsund | Telemark | Rymteland | 914 ± 6 (Pedersen and Maaløe 1990) | Lyngdal | 930 ± 28 (Pedersen and Falkum 1975) | ages overlap | 2 |
| Flesberg | Telemark | Bjertnes | 908 ± 12* | No granite exposed | | – | 2 |
| Østfold | Idefjorden | Halvorsrød | 902.9 ± 1.7* | Iddefjord | 918 ± 7 (Pedersen and Maaløe 1990) | 6 | 2 |
| Østfold | Idefjorden | Karlshus | 906.3 ± 5.9 (Müller et al. 2017) | Iddefjord | 918 ± 7 (Pedersen and Maaløe 1990) | ages overlap | 2 |
| Østfold | Idefjorden | Vintergruben | 908.9 ± 1.4 (Müller et al. 2017) | Iddefjord | 918 ± 7 (Pedersen and Maaløe 1990) | ages overlap | 2 |
| Halland | Idefjorden | Grebbestad | 921.8 ± 3.4 (Müller et al. 2017) | Bohus | 922 ± 5 (Eliasson and Schöberg 1991) | ages overlap | 2 |
| Østfold | Idefjorden | Herrebøkasa | 910.1 ± 5.3* | Bohus | 922 ± 5 (Eliasson and Schöberg 1991) | 3 | 2 |
| Kristiansand | Bamble | Flekkerøy | 915.4 ± 1.6 (Müller et al. 2017) | No granite exposed | – | – | 2 |
| Kristiansand | Bamble | Randesund | 918.1 ± 2.9* | No granite exposed | – | – | 2 |
| Kristiansand | Bamble | Salbostat | 921.6 + 4.4/-5.1* | No granite exposed | – | – | 2 |
| Eastern segment | Eastern Segment | Riddaho | 941.6 ± 1.4 (Romer and Smeds 1996) | No granite exposed | – | – | |
| Halland | Idefjorden | Skuleboda | 984.3 ± 6.4 (Romer and Smeds 1996) | No granite exposed | 922 ± 5 (Eliasson and Schöberg 1991) | 51 | |
| Haugesund | Telemark | Tors gruve | 991.6 ± 3.6 (Müller et al. 2017) | No granite exposed | – | – | |
| Fyresdal | Telemark | Bjønnetjønn | 984 ± 12* | Fyresdal | 861 ± 50 (Venugopal, 1970) | 61 | |

* This study.

**Table 7**
Characteristics of Group 1 and 2 pegmatites. Pegmatite of both groups belong have chemical NYF affinity.

| Group | Age range (Ma) | Lithotectonic unit | Tectonic setting | Deformation grade of pegmatite | Host rock | Pegmatite zonation | Pegmatite class (Černý and Ercit 2005) |
|---|---|---|---|---|---|---|---|
| Group 1 | 1100–1030 | Bamble, Idefjorden | Transpressional regime | Slightly deformed | Biotite-, amphibole-biotite gneiss, amphibolite | Weakly zoned | Abyssal, MS-rEL-REE to primitive rEL-REE predominantly of the allanite-(Ce)-monazite-(Ce) subtype |
| Group 2 | 930–890 | Telemark, Bamble, Idefjorden | Extensional regime | Undeformed | Amphibolite, amphibole-biotite gneiss | Distinct Zoned | Abyssal to evolved rEL-REE of the gadonlite-(Y) subtype |

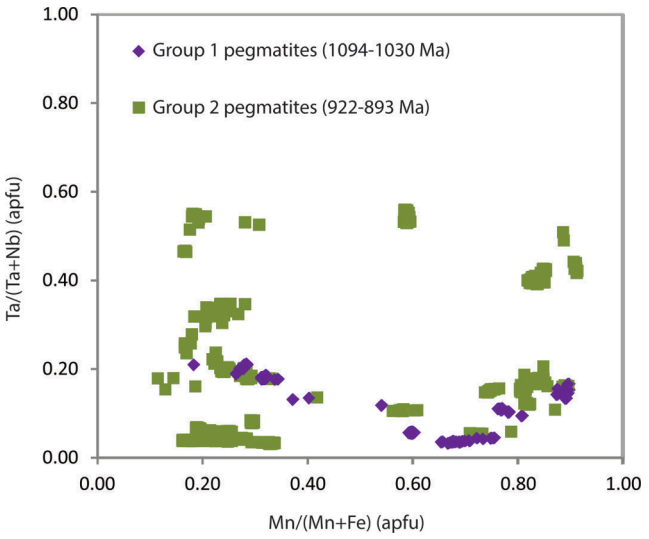


**Fig. 10.** Columbite group mineral chemistry (apfu) of the different age groups. Group 2 contains the most evolved columbite group minerals. Group 2 follows two separate evolution trends like the trends described in Černy (1989). The left trend is common for columbite group minerals crystallized in F-poor conditions in beryl type pegmatites, whereas the right trend represents columbite group minerals crystallized in F-rich conditions in complex lepidolite type pegmatites.

amphibolites and to lesser extent in biotite gneisses, whereas Group 1 pegmatites occur preferentially in biotite-amphibole and biotite gneisses of granodioritic composition. Third, Group 1 pegmatites are often related to shear zones (Henderson and Ihlen, 2004; Müller et al., 2015), whereas but Group 2 pegmatites seem to be unrelated to major structures. Instead, Group 2 pegmatites occur commonly in large-scale amphibolite bodies such as the Iveland-Gautestad complex (host of the Evje-Iveland pegmatites) and the Nissedal supracrustal complex (host of the Tørdal pegmatites). The distribution of Group 2 pegmatites seems to be controlled predominantly by the regional distribution of amphibolite massifs.

The amphibolite-bound Group 2 pegmatite occurrence seems to be related to the rheological and petrophysical differences between amphibolites and granitic rocks. Field observations indicate that amphibolite reacted brittle to semi-brittle forming extensional structures into which partial melts drain preferentially, whereas the more ductile surrounding granitic gneisses provided only little possibility for partial melts to collect in pressure shadows.

Low-degree partial melts of amphibolites and diorites have granitic compositions with high contents of $SiO_2$, $K_2O$, $Na_2O$ and $H_2O$ and low contents of $Al_2O_3$, CaO, $Fe_2O_3$, MgO and $TiO_2$ (e.g., Beard and Lofgren, 1991; Green et al., 2016; Palin et al. 2016; Wolf and Wyllie, 1994; Wyllie and Wolf, 1993). Hornblende and biotite are the most abundant hydrous phase in these rocks. Their breakdown releases REE and F, which define the hallmark geochemical fingerprint of NYF pegmatite melts (Černý, 1991a). Intermediate to mafic lithologies, however, have generally higher solidus temperatures than silica-rich granites, granitic gneisses and metasediments. For $H_2O$-saturated conditions, granitic rocks and metasediments of near eutectic compositions start to melt at about 640 °C for pressures of 4 kbar (the approximate pressure of Group 2 pegmatite formation; Müller et al., 2015), whereas amphibolites and diorites start to melt in the range of 680–710 °C for 4–5 kbar (e.g., Palin et al., 2016; Stuck and Diener, 2018; Tuttle and Bowen, 1958). Partial melting of S-type granites and metasediments, however, yields LCT type pegmatite melts (Černý, 1991a). Such LCT-type pegmatites are not found in the Sveconorwegian orogen. Pegmatites of the Sveconorwegian orogen predominantly have NYF-type signatures (Müller et al., 2015, 2017). Fig. 12 shows textural examples of pegmatite melt segregation and movement in metagabbro at different scales exposed in the Kleppe quarry in the center of the Tørdal pegmatite field.

Migmatites are widespread in the high-grade metamorphic units of the Sveconorwegian orogen, i.e., the Agder migmatite domain in the Telemark lithotectonic unit (Falkum, 1966), migmatite gneisses of the Gothenburg-Halmstad area in the southern part of the Idefjorden unit (e.g., Möller et al., 2015), and the migmatite complex of the Risør area (Starmer, 1969). These felsic granitic gneisses and metasediments locally show migmatite leucosomes (usually $< 10$ m$^3$) with pegmatitic textures, but they did not produce large (>1000 m$^3$) NYF type pegmatites. Instead, NYF-type pegmatites are spatially related to amphibolites and I-type granites. Even though both gneisses and amphibolites have been affected by melting, the chemical signature and spatial distribution of pegmatites indicate (i) that gneisses did not allow for the collection of large melt volumes, whereas the amphibolites allowed for the collection of local melts in pressure shadows and (ii) the amphibolites contributed to the pegmatite melts (see also Müller et al., 2015, 2017). The melting of the amphibolites may have been facilitated by fluids or melt from the more silicic wall rocks or by $CO_2$ released from the crystallization of the mafic magmas that underplated the orogen on a regional scale around 920 Ma (Fig. 11; Vander Auwera et al., 2003, 2014; Andersen et al., 2007b; Slagstad et al., 2018; Granseth et al., 2020). The release of $CO_2$ destabilized mica and amphibole due to a series of dehydration reactions (Touret and Hartel, 1990).

### 5.4. Pegmatite emplacement in amphibolite

Amphibolites are more rigid at mid-crustal depth than quartz-K-feldspar-mica rich granitic gneisses and metasedimentary rocks (e.g., Berger and Stünitz, 1996; Ishii et al., 2007; Passchier and Trouw, 1996). As a consequence, shearing results in ductile deformation of the granitic gneisses and fracturing of the amphibolite bodies. Fluids and partial melts will concentrate in these fractures and pressure shadows at the contacts between amphibolites and more felsic rocks. Near-solidus temperature fluids released from the crystallizing mafic melts emplaced in the lower crust may reduce melting temperatures. The destabilization of amphibole will release significant amounts of F, which in turn may decrease the solidus temperature and the viscosity of the melt (e.g., London, 1987), allowing for the extraction of melt already for very low degrees of partial melting (e.g., Baker and Vaillencourt, 1995). The collection of locally produced melt in fractures in amphibolite also explains the NYF character of the pegmatites. In contrast, partial melts in the nearby granitic gneisses (which would have LCT character) may

not have collected in veins, but crystallized locally within the gneisses and may have been affected by subsequent deformation and recrystallization. Such a contrasting behavior of mafic and felsic rocks, would explain not only the distribution of the pegmatites, but also the NYF character of the pegmatites and the absence of LCT pegmatites in the gneisses. The dominate role of contrasting rheological behavior for the distribution of pegmatites is known on a wide range of scales.

As an outcrop scale example, a road cut at Remmen near Halden (Idefjorden lithotectonic unit) exposes several amphibolite mega boudins embedded in biotite gneiss (Fig. 13). The outcrop, its tectonic setting and age, are described in detail by Narum et al. (2022). While the banded biotite gneiss is ductilely deformed, the amphibolite was fractured during compressional deformation. The small-scale, extensional fractures host different generations of pegmatites containing monazite-(Ce) and allanite-(Ce) (NYF-type pegmatites). Except for a first generation of veins, which are probably of Gothian age (1549 Ma), the main pegmatites formed during several stages between ca. 1041 and 1033 Ma (Narum et al., 2022). Those located in the surrounding migmatitic gneiss also record the deformation and folding of the host gneiss.

A similar rheology-controlled pegmatite distribution on the km-scale has been shown by Lindroos et al. (1996) for NYF pegmatites in the Kimito pegmatite field of SW Finland, which is located in a major late-orogenic Svecofennian shear zones. Major pegmatite bodies are hosted in little deformed gabbros, whereas the sheared wall rocks of the gabbros do not host significant pegmatites (Fig. 2 in Lindroos et al., 1996).

### 5.5. *The Sveconorwegian pegmatite formation in the context of the Grenville–Sveconorwegian orogeny*

The Late Mesoproterozoic Grenville–Sveconorwegian orogen resulted from multiple collision, accretion, and re-amalgamation events of fragmented and attenuated crustal blocks between Baltic, Laurentia and Amazonia, eventually leading to the assembly of the supercontinent Rodinia (e.g., Li et al., 2008, Slagstad et al., 2017). Attempts of correlations between the Grenville and Sveconorwegian orogens based on paleomagnetic data (e.g., Evans, 2013) and on the comparison of the orogenic architecture (e.g., Bingen et al., 2008c; Möller et al., 2015; Romer et al., 1996). These attempts revealed that tectonothermal events along the>5000 km long Sveconorwegian and the Grenville orogens do not strictly correlate and were rather formed by discrete, regional-restricted tectonothermal events. Similar processes operated at different time and not all tectonic event present in one segment of the belt also occur in other segments of the belt. The Grenville orogen is considered to be a hot and long-lived orogen (e.g. Rivers, 2008) with abundant evidence for partial melting (e.g. Indares et al., 2008; Jannin et al., 2018; Slagstad et al., 2004; Timmermann et al., 2002; Turlin et al., 2018) and mafic magmatism (Rivers and Corrigan, 2000). The Grenville orogeny *sensu stricto* includes two orogenic phases, namely the (i) Ottawan phase (ca. 1090–1020 Ma) and the (ii) Rigolet phase (ca. 1005–960 Ma; Carr et al., 2000; Hynes and Rivers, 2010; Rivers et al., 2012; Tucker and Gower, 1994) The Sveconorwegian orogeny includes four events: the 1.14–1.08 Ga Arendal, 1.05–0.98 Ga Agder (main compression phase), 980–970 Ma Falkenberg and 960–900 Ma Dalane phases (post-collisional magmatism; Bingen et al., 2008b). The Arendal event recorded in the Sveconorwegian Bamble lithotectonic unit correlates well with Grenville events in the Frontenac terrane, Adirondacks and Quebec where is associated with bimodal magmatism, anorthosites, and high grade metamorphism (e.g. Corfu and Easton, 1997).

Grenville pegmatites dominantly have abyssal and NYF-type character and are mainly known from the central and northern parts of the Grenville province (Ayres and Černý, 1982; Bradley et al., 2017; Černý, 1991b; Ercit, 2005; Fowler and Doig, 1983; Groulier et al., 2018; Lentz, 1996; Masson and Gordon, 1981; Turlin et al., 2017). These pegmatites have ages between ca. 1090 and 980 Ma, although most of them were emplaced at 1010 to 980 Ma (Supplementary Material SM04). For, comparison, the Ottawan peak of metamorphism climaxed between ca. 1070 and 1050 Ma (Lasalle et al., 2014; Lasalle and Indares, 2014; Turlin et al., 2018), i.e., before most Grenville pegmatites formed, whereas the Rigolet orogenic phase occurred at ca. 1005 to 960 Ma, reaching peak conditions of ca. 12.5 to 15 kbar and ca. 815–850 °C

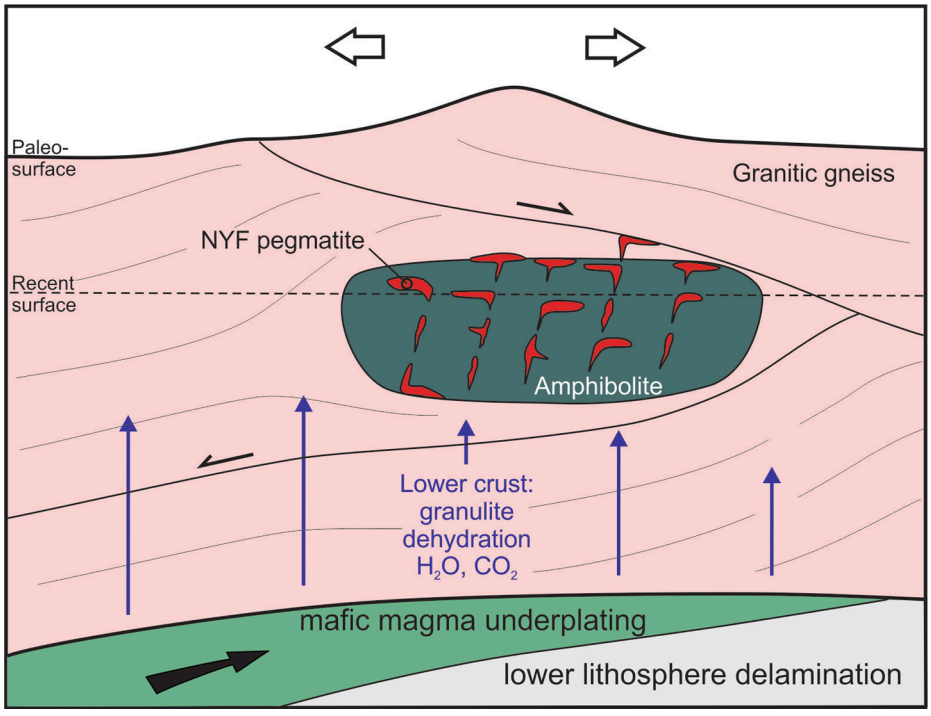


**Fig. 11.** Generic model for the partial melting of amphibolites and Group 2 pegmatite formation as a result of mafic magma underplating, which accounts for high heat flow, volatile input from the crystallizing mafic rocks, and dehydration melting of the lower (granulitic) crust. Local melts concentrate in fractures in amphibolites that are less ductile than the surrounding granitic gneisses.

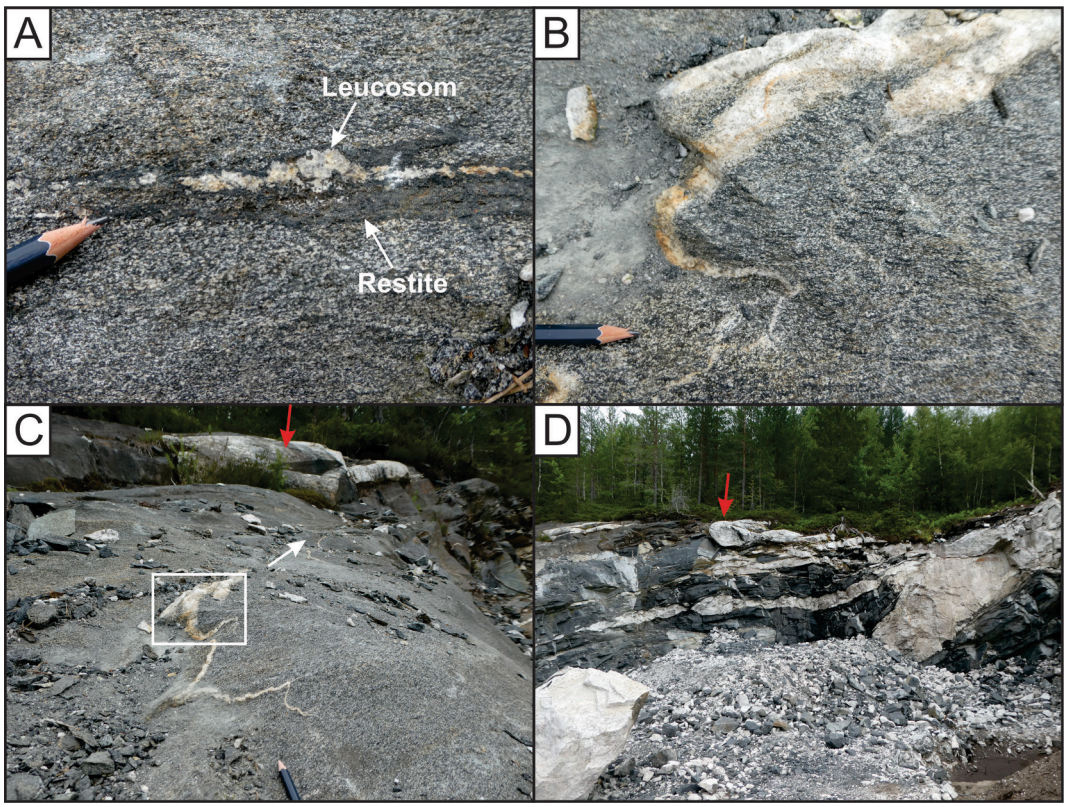


**Fig. 12.** (A) Leucocratic veinlet bordered by dark, restitic, amphibole-enriched metagabbro. The veinlet continues and widens up to a pegmatitic vein (B), which leads into a larger (meter-sized) pegmatite body (red arrow in C). (D) View of the Kleppe quarry in the center of the Tørdal pegmatite field were the photographs in (A) to (C) were taken. The red arrow corresponds to the pegmatite shown in (C). The boudinage of the pegmatite sheet in the lower part of the wall indicates extensional tectonics during melt emplacement. (For interpretation of the references to colour in this figure legend, the reader is referred to the web version of this article.)

(Hynes et al., 2000; Jannin et al., 2018; Jordan et al., 2006; Krogh, 1994; Rivers, 2008, 2009; Rivers et al., 1989, 2012; Van Gool et al., 2008), overlapping with the age of most Grenville pegmatites. The geological, geochemical, and geochronological evidence provided for NYF pegmatites of the Grenville orogen favours an anatectic origin, including partial melting of mid-crustal lithologies coupled with fractionation (Fowler and Doig 1983; Lentz, 1991, 1996; Turlin et al., 2017).

The Grenville pegmatite formation overlaps partially with the Sveconorwegian Group 1 event but the Grenville peak clearly postdates the Norwegian Group 1 peak by about 30 Ma. This implies that similar orogenic settings and tectono-metamorphic conditions favourable for NYF pegmatite formation were not coeval in the Grenville and Sveconorwegian section of the orogen. However, the predominant process of pegmatite formation is anatectic melting (e.g. Turlin et al., 2017) as postulated for the majority of Sveconorwegian pegmatites.

## 6. Conclusions

Pegmatite formed mainly during two periods of the Sveconorwegian orogeny: the *syn*-orogenic Group 1 pegmatites (1100–1030 Ma) and post-orogenic Group 2 pegmatites (930–890 Ma). Group 1 pegmatites are confined to the lithotectonic unit of the Bamble and Idefjorden lithotectonic units, whereas Group 2 pegmatites also occur and are most widespread in the Telemark unit. A few isolated pegmatite bodies with crystallization ages between 997 and 940 Ma are recorded between these two groups in the different parts of the Sveconorwegian orogen.

Group 1 pegmatites formed after granulite-facies peak metamorphism and are related to transpressional-activated shear zones transecting the Bamble, Kongsberg and Idefjorden lithotectonic units. This regional metamorphism resulted in crustal melting, in particular along shear zones that also served as pathways for the melts.

Group 2 pegmatites were emplaced in an extensional regime. The pegmatite emplacement followed a period of extensive hornblende-biotite granite magmatism. Underplating of mafic magma provided the heat source for this extensive granitic magmatism (e.g. Andersen et al., 2007b; Slagstad et al., 2018; Granseth et al., 2020) and for Group 2 pegmatite melts. Pegmatites in the Telemark and Idefjorden lithotectonic units are 10 to 20 m.y. younger than the granites, whereas the Group 2 Østfold pegmatites are coeval with adjacent hornblende-biotite granitic plutons. The Iddefjord and Bohus granites could be the source of the Østfold pegmatites or could have provided the heat for crustal melting forming the pegmatites. Group 2 pegmatites related to the Iddefjord and Bohus granites and those unrelated to granites do not differ in mineralogy and chemistry. The major reason why pegmatites are predominantly hosted by amphibolite is the brittle to semi-brittle behavior of amphibolite producing local stress minima toward which fluids and melts migrated. The two pegmatite Groups formed in different tectonic settings by different processes, which indicates that the main control on compositional variation of pegmatitic melt is the source rather than the mobilization process.

The late Mesoproterozoic Grenville province as the part of the Grenville–Sveconorwegian orogenic belt hosts abundant abyssal and NYF-type pegmatites as the Sveconorwegian part. Pegmatites in the Grenville province predominantly have ages around 980 to 1010 Ma, i.e., are about 30 Ma younger than corresponding Group 1 pegmatites in the Sveconorwegian orogen.

## CRediT authorship contribution statement

**N. Rosing-Schow:** Investigation, Conceptualization, Writing –

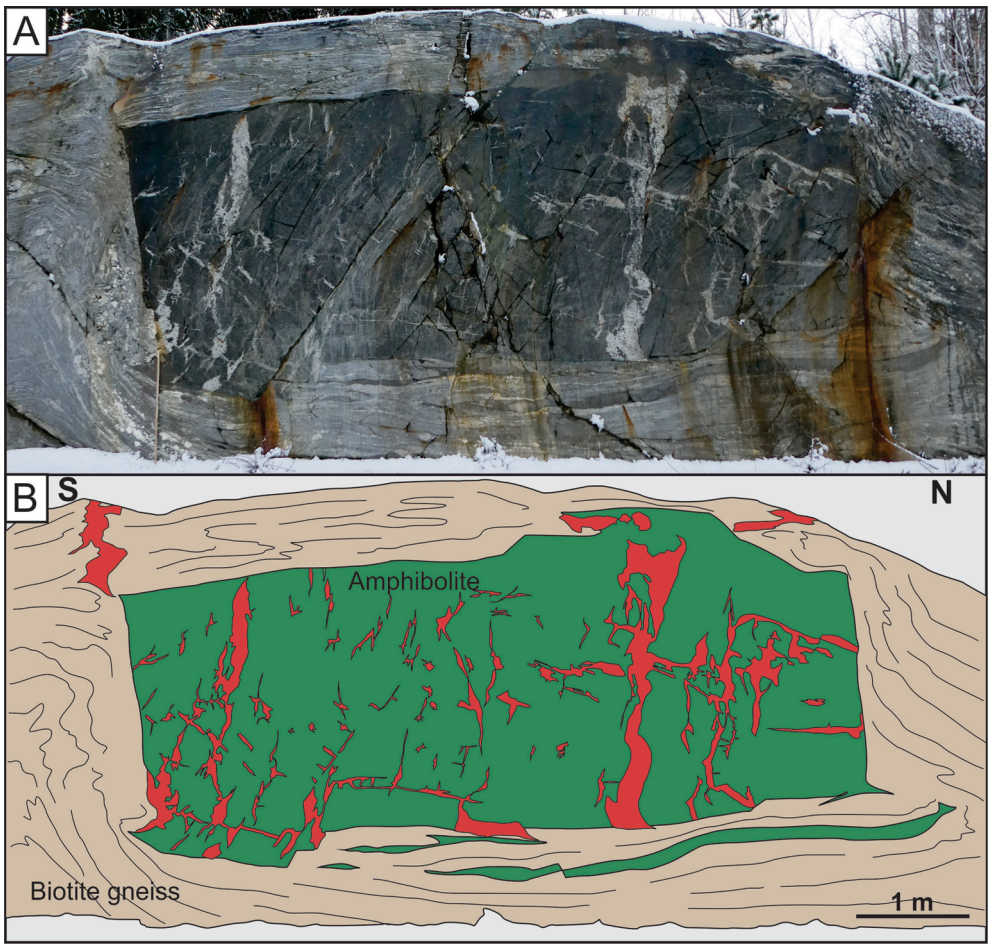


**Fig. 13.** Road cut at Remmen near Halden, Norway, showing a large, rectangular, predominantly brittle deformed amphibolite boudin (green) embedded in ductile deformed migmatitic biotite gneiss (brown). Small pegmatites (red) emplaced in extensional structures mainly within the amphibolite. (For interpretation of the references to colour in this figure legend, the reader is referred to the web version of this article.)

original draft. **R.L. Romer:** Conceptualization, Methodology, Writing – review & editing. **A. Müller:** Supervision, Conceptualization, Project administration, Resources, Funding acquisition, Writing – review & editing. **F. Corfu:** Methodology, Writing – review & editing. **R. Škoda:** Methodology, Writing – review & editing. **H. Friis:** Formal analysis, Validation, Writing – review & editing.

## Declaration of Competing Interest

The authors declare the following financial interests/personal relationships which may be considered as potential competing interests: [Axel Muller reports financial support was provided by European Commission.].

## Data availability

All data discussed are accessible through the Supplementary Materials

## Acknowledgements

We thank Alf Olav Larsen (mineral collector), Tor Sigvald Johansen (Natural History Museum and Botanical Garden, University of Agder) and Arild Omestad (mineral collector and dealer) for providing some of the columbite and monazite samples (see Supplementary Material SM02). We are grateful to Muriel Erambert for support in acquiring the EPMA data. We are thankful to Bernard Bingen and Trond Slagstad for thoughtful and detailed reviews and Frances Westall for thoughtful editorial handling. This study was funded by a Ph.D. stipend awarded to the first author by the Natural History Museum of Oslo, University of Oslo, Norway und the umbrella of the European Commission's Horizon 2020 innovation programme under grant agreement No 869274, project GREENPEG New Exploration Tools for European Pegmatite Green-Tech Resources.

## Appendix A. Supplementary material

Supplementary data to this article can be found online at https://doi.org/10.1016/j.precamres.2022.106944.

## References

Åhäll, K.I., Cornell, D.H., Armstrong, R., 1998. Ion probe zircon dating of metasedimentary units across the Skagerrak: new constraints for early Mesoproterozoic growth of the Baltic Shield. Precambr. Res. 87, 117–134.
Andersen, T., 1997. Radiogenic isotope systematics of the Herefoss granite, South Norway: An indicator of Sveconorwegian (Grenvillian) crustal evolution in the Baltic Shield. Chem. Geol. 135, 139–158.
Andersen, T., Andresen, A., Sylvester, A.G., 2002. Timing of late- to post-tectonic Sveconorwegian granitic magmatism in South Norway. Norges Geol. Unders. Bull. 440, 5–18.
Andersen, T., Graham, S., Sylvester, A.G., 2007a. Timing and tectonic significance of Sveconorwegian A-type granitic magmatism in Telemark, southern Norway: new results from laser-ablation ICPMS U-Pb dating of zircon. Norges Geol. Unders. Bull. 447, 17–31.
Andersen, T., Griffin, W.L., Sylvester, A.G., 2007b. Sveconorwegian crustal underplating in southwestern Fennoscandia: LAM-ICPMS U-Pb and Lu–Hf isotope evidence from granites and gneisses in Telemark, southern Norway. Lithos 93, 273–287.

Austin Hegardt, E., 2010. Pressure, Temperature and Time Constraints on Tectonic Models of Southwestern Sweden. In: Department of Earth Sciences. University of Gothenburg, pp. 1–91.
Austin Hegardt, E., Cornell, D.H., Hellström, F.A., Lundqvist, I., 2007. Emplacement age of the mid-Proterozoic Kungsbacka Bimodal Suite, SW Sweden. GFF 129, 227–234.
Ayres, L.D., Černý, P., 1982. Metallogeny of granitoid rocks in the Canadian Shield. Can. Mineral. 20, 439–536.
Baadsgaard, H., Chaplin, C., Griffin, W.L., 1984. Geochronology of the Gloserheia pegmatite, Froland, southern Norway. Nor. Geol. Tidsskr. 64, 111–119.
Baker, D.R., Vaillencourt, J., 1995. The low viscosities of F + $H_2O$-bearing granitic melts and implications for melt extraction and transport. Earth Planet. Sci. Lett. 132, 199–211.
Beard, J.S., Lofgren, G.E., 1991. Dehydration melting and water-saturated melting of basaltic and andesitic greenstones and amphibolites at 1, 3 and 6–9 kb. J. Petrol. 32, 365–401.
Berger, A., Stünitz, H., 1996. Deformation mechanisms and reaction of hornblende: examples from the Bergell tonalite (Central Alps). Tectonophysics 257, 149–174.
Bergstøl, S., Juve, G., 1988. Scandian ixiolite, pyrochlore and bazzite in granite pegmatite in Tørdal, Telemark, Norway. A contribution to the mineralogy and geochemistry of scandium and tin. Mineral. Petrol. 38, 229–243.
Bingen, B., Davis, W.J., Hamilton, M.A., Engvik, A.K., Stein, H.J., Skår, Ø., Nordgulen, Ø., 2008a. Geochronology of high-grade metamorphism in the Sveconorwegian belt, S. Norway: U-Pb, Th-Pb and Re-Os data. Nor. J. Geol. 88, 13–42.
Bingen, B., Nordgulen, Ø., Viola, G., 2008b. A four-phase model for the Sveconorwegian orogeny, SW Scandinavia. Nor. J. Geol. 88, 43–72.
Bingen, B., Andersson, J., Söderlund, U., Möller, C., 2008c. The Mesoproterozoic in the Nordic countries. Episodes 31, 1–6.
Bingen, B., Viola, G., 2018. The early-Sveconorwegian orogeny in southern Norway: tectonic model involving delamination of the sub-continental lithospheric mantle. Precambr. Res. 313, 170–204.
Bingen, B., Viola, G., Möller, C., Vander Auwera, J., Laurent, A., Yi, K., 2021. The Sveconorwegian orogeny. Gondw. Res. 90, 273–313.
Bjørlykke, H., Burger, A.J., 1962. The age of the Bjertnes uraninite. Nor. Geol. Tidsskr. 42, 187–190.
Bolle, O., Diot, H., Vander Auwera, J., Dembele, A., Schittekat, J., Spassov, S., Ovtcharova, M., Schaltegger, U., 2018. Pluton construction and deformation in the Sveconorwegian crust of SW Norway: magnetic fabric and U-Pb geochronology of the Kleivan and Sjelset granitic complexes. Precambr. Res. 305, 247–267.
Bradley, D.C., McCauley, A.D., Stillings, L.M., 2017. Mineral-deposit model for lithium-cesium-tantalum pegmatites. U.S. Geological Survey Scientific Investigations Report 2010–5070–O, 48 p., Doi: 10.3133/sir201050700.
Bue, E.P., 2005. Age and origin of the Mesoproterozoic basement of the Nesodden Peninsula, SE Norway. A geochronological and isotopic study. University of Oslo, p. 88 pp.. MSc thesis.
Bybee, G.M., Ashwal, L.D., Shirey, S.B., Horan, M., Mock, T., Andersen, T.B., 2014. Pyroxene megacrysts in Proterozoic anorthosites: Implications for tectonic setting, magma source and magmatic processes at the Moho. Earth Planet. Sci. Lett. 389, 74–85.
Carr, S.D., Easton, R.M., Jamieson, R.A., Culshaw, N.G., 2000. Geologic transect across the Grenville orogen of Ontario and New York. Can. J. Earth Sci. 37, 193–216. https://doi.org/10.1139/e99-074.
Černý, P., 1991a. Rare-element granitic pegmatites, Part I. Anatomy and internal evolution of pegmatite deposits. Geosci. Can. 18, 49–67.
Černý, P., 1991b. Rare-element granitic pegmatites, Part II. Regional to global environments and petrogenesis. Geosci. Can. 18, 68–81.
Černý, P., Ercit, T.S., 2005. The classification of granitic pegmatites revisited. Can. Mineral. 43, 2005–2026.
Černý, P., London, D., Novák, M., 2012. Granitic pegmatites as reflections of their sources. Elements 8, 289–294.
Coint, N., Slagstad, T., Roberts, N.M.W., Marker, M., Røhr, T., Sørensen, B.E., 2015. The Late Mesoproterozoic Sirdal Magmatic Belt, SW Norway: Relationships between magmatism and metamorphism and implications for Sveconorwegian orogenesis. Precambr. Res. 265, 57–77.
Cooper, M.A., Abdu, Y.A., Ball, N.A., Černý, P., Hawthorne, F.C., Kristiansen, R., 2012. Aspedamite, ideally $\square_{12}(Fe^{3+}, Fe^{2+})_3Nb_4[Th(Nb, Fe^{3+})_{12}O_{42}]\{(H2O),(OH)\}12$, a new heteropolyniobate mineral species from the Herrebøkasa quarry, Aspedammen, Østfold, Southern Norway: Description and crystal structure. Can. Mineral. 50, 793–804.
Corfu, F., Andersen, T.B., 2002. U-Pb ages of the Dalsfjord Complex, SW-Norway, and their bearing on the correlation of allochthonous crystalline segments of the Scandinavian Caledonides. Int. J. Earth Sci. 91, 955–963.
Corfu, F., Easton, R.M., 1997. Sharbot Lake terrane and its relationships to Frontenac terrane, Central Metasedimentary Belt, Grenville Province: new insights from U-Pb geochronology. Can. J. Earth Sci. 34, 1239–1257.
Cosca, M.A., Mezger, K., Essene, E.J., 1998. The Baltica-Laurentia connection: Sveconorwegian (Granvillian) metmaorphism, cooling, and unroofing in the Bamble Sector, Norway. J. Geol. 106, 539–552.
Davis, D.W., Blackburn, C.E., Krogh, T.E., 1982. Zircon U-Pb ages from the Wabigoon-Manitou Lakes region, Wabigoon Subprovince, northwest Ontario. Can. J. Earth Sci. 19, 254–266.
deHaas, G.J.I.M., Nijland, T.G., Andersen, T., Corfu, F., 2002. New constraints on the timing of deposition and metamorphism in the Bamble sector, south Norway: zircon and titanite U-Pb data from the Nelaug area. GFF 124, 73–78.
Dons, J.A., Broch, O.A., Liestøl, G.B., Siggerud, T., 1960. The stratigraphy of supracrustal rocks, granitization and tectonics in the Precambrian Telemark area Southern Norway. Norges Geologiske Undersøkelse, Oslo, pp. 1-30.
Druguet, E., Hutton, D.H.W., 1998. Syntectonic anatexis and magmatism in a mid-crustal transpressional shear zone: an example from the Hercynian rocks of the eastern Pyrenees. J. Struct. Geol. 20, 905–916.
Eliasson, T., Schöberg, H., 1991. U-Pb dating of the post-kinematic Sveconorwegian (Grenvillian) Bohus granite, SW Sweden - evidence of restitic zircon. Precambr. Res. 51, 337–350.
Engvik, A.K., Mezger, K., Wortelkamp, S., Bast, R., Corfu, F., Korneliussen, A., Ihlen, P., Bingen, B., Austrheim, H., 2011. Metasomatism of gabbro – mineral replacement and element mobilization during the Sveconorwegian metamorphic event. J. Metam. Geol. 29, 399–423.
Engvik, A.K., Bingen, B., Solli, A., 2016. Localized occurrences of granulite: P-T modeling, U-Pb geochronology and distribution of early-Sveconorwegian high-grade metamorphism in Bamble, South Norway. Lithos 240–243, 84–103.
Ercit, T.S., 2005. REE-enriched granitic pegmatites. Short Course Notes – Geological Association of Canada 17, 175–199.
Evans, D.A.D., 2013. Reconstructing pre-Pangean supercontinents. Geol. Soc. Am. Bull. 125, 1735–1751.
Falkum, T., 1966. Structural and petrol ogical investigations of the Precambrian metamorphic and igneous charnockite and migmatite complex in the Flekkefjord area, Southern Norway. Nor. Geol. Unders. 242, 19–25.
Falkum, T., 1985. Geotectonic evolution of southern Scandinavia in the light of a late-Proterozoic plate-collision. In: Tobi, A.C., Touret, J.L.R. (Eds.), the Deep Proterozoic Crust in the North Atlantic Provinces. Springer, Netherlands, pp. 309–322.
Field, D., Råheim, A., 1981. Age relationships in the Proterozoic high-grade gneiss regions of southern Norway. Precambr. Res. 14, 261–275.
Fowler, A.D., Doig, R., 1983. The age and origin of Grenville Province uraniferous granites and pegmatites. Can. J. Earth Sci. 20, 92–104.
Fuchsloch, W.C., Nex, P.A.M., Kinnaird, J.A., 2018. Classification, mineralogical and geochemical variations in pegmatites of the Cape Cross-Uis pegmatite belt, Namibia. Lithos 296, 79–95.
Gellein, J., 2003. Gravimetrisk residualkart, Arendal. Norges Geologiske Undersøkelse, Trondheim. <https://www.ngu.no/sokkelkart/Arendal_200.jpg> Accessed 10 January 2022.
Gellein, J., 2007. Gravimetrisk residualkart, Skien. Norges Geologiske Undersøkelse, Trondheim. <https://www.ngu.no/sokkelkart/Skien_200.jpg> Accessed 10 January 2022.
Granseth, A., Slagstad, T., Coint, N., Roberts, N.M.W., Røhr, T.S., Sørensen, B.E., 2020. Tectonomagmatic evolution of the Sveconorwegian orogen recorded in the chemical and isotopic compositions of 1070–920 Ma granitoids. Precambr. Res. 340, 105527.
Green, E.C.R., White, R.W., Diener, J.F.A., Powell, R., Holland, T.J.B., Palin, R.M., 2016. Activity-composition relations for the calculation of partial melting equilibria in metabasic rocks. J. Metam. Geol. 34, 845–869. https://doi.org/10.1111/jmg.12211.
Groulier, P.-A., Indares, A., Dunning, G., Moukhsil, A., Jenner, G., 2018. Syn-orogenic magmatism over 100 m.y. in high crustal levels of the central Grenville Province: Characteristics, age and tectonic significance. Lithos 312–313, 128–152. https://doi.org/10.1016/j.lithos.2018.04.025.
Henderson, I., Ihlen, P.M., 2004. Emplacement of polygeneration pegmatites in relation to Sveconorwegian contractional tectonics: examples from southern Norway. Precambr. Res. 133, 207–222.
Høy, I., 2016. Sveconorwegian Magmatic and Metamorphic Evolution of Southwestern Norway. University of Oslo, Oslo, p. 132. Master thesis,.
Hutton, D.H.W., Reavy, R.J., 1992. Strike-slip tectonics and granite petrogenesis. Tectonics 11, 960–967.
Hynes, A., Rivers, T., 2010. Protracted continental collision - evidence from the Grenville Orogen. Can. J. Earth Sci. 47, 591–620. https://doi.org/10.1139/E10-003.
Hynes, A., Indares, A., Rivers, T., Gobeil, A., 2000. Lithoprobe line 55: integration of outof-plane seismic results with surface structure, metamorphism, and geochronology, and the tectonic evolution of the eastern Grenville Province. Canandian Journal of Earth Sciences 37, 341–358. https://doi.org/10.1139/e99-076.
Ihlen, P.M., Müller, A., 2009. Rare-element pegmatites in the Sveconorwegian orogen (0.9-1.1 Ga) of southern Norway. Estudos Geològicos 19.
Indares, A., White, R.W., Powell, R., 2008. Phase equilibria modelling of kyanite-bearing anatectic paragneisses from the central Grenville Province. J. Metam. Geol. 26, 815–836.
Ishii, K., Kanagawa, K., Shigematsu, N., Okudaira, T., 2007. High ductility of K-feldspar and development of granitic banded ultramylonite in the Ryoke metamorphic belt, SW Japan. J. Struct. Geol. 29, 1083–1098.
Jaffey, A.H., Flynn, K.F., Glendenin, L.E., Bentley, W.C., Essling, A.M., 1971. Precision measurement of half-lives and specific activities of U-235 and U-238. Phys. Rev. C 4, 1889–1906.
Jannin, S., Gervais, F., Moukhsil, A., Augland, L.E., Crowley, J.L., 2018. Déformations tardi grenvilliennes dans la Ceinture parautochtone (Province de Grenville centrale): contraintes géochronologiques par couplage de méthodes U/Pb de haute résolution spatiale et de haute précision. Can. J. Earth Sci. 55, 406–435.
Jarosewich, E., Boatner, L.A., 1991. Rare-element reference samples for electron-microprobe. Geostand. Newslett. 15, 397–399.
Jensen, E., Corfu, F., 2016. The U-Pb age of the Finse batholith, a composite bimodal Sveconorwegian intrusion. Nor. J. Geol. 96, 171.
Jercinovic, M.J., Williams, M.L., 2005. Analytical perils (and progress) in electron microprobe trace element analysis applied to geochronology: background acquisition, interferences, and beam irradiation effects. Am. Mineral. 90, 526–546.

Jordan, S.L., Indares, A., Dunning, G., 2006. Partial melting of metapelites in the Gagnon terrane below the high-pressure belt in the Manicouagan area (Grenville Province): pressure–temperature (P–T) and U-Pb age constraints and implications. Can. J. Earth Sci. 43, 1309–1329. https://doi.org/10.1139/E06-038.
Juve, G., Bergstøl, S., 1997. Granittpegmatitter i Tørdal. Telemark. Kongsberg Mineralsymposium. Norsk Bergverksmuseum Skrift 12, 56–57.
Karlsson, A.K.-O., Zack, T., 2017. In situ Rb-Sr dating by LA-ICP-MS/MS, a novel and powerful method for pegmatite geochronology. PEG2017 – Proceedings of the 8th Symposium on Granitic Pegmatites, Kristiansand, 13-15 June 2017. Abstracts and Proceedings of the Geological Society of Norway 2017-2, 62-63.
Konzett, J., Schneider, T., Nedyalkova, L., Hauzenberger, C., Melcher, F., Gerdes, A., Whitehouse, M., 2018. Anatectic granitic pegmatites from the Eastern Alps: A case of variable rare-metal enrichment during high-grade regional metamorphism - I: Mineral assemblages, geochemical characteristics, and emplacement ages. Can. Mineral. 56, 555–602.
Krogh, T.E., 1973. Low-contamination method for hydrothermal decomposition of zircon and extraction of U and Pb for isotopic age determinations. Geochim. Cosmochim. Acta 37, 485–494.
Krogh, T.E., 1982. Improved accuracy of U-Pb zircon ages by the creation of more concordant systems using an air abrasion technique. Geochim. Cosmochim. Acta 46, 637–649.
Krogh, T.E., 1994. Precise U-Pb ages for Grenvillian and pre-Grenvillian thrusting of Proterozoic and Archean metamorphic assemblages in the Grenville Front tectonic zone, Canada. Tectonics 13, 963–982. https://doi.org/10.1029/94TC00801.
Kullerud, L., Machado, N., 1991. End of a controversy: U-Pb geochronological evidence for significant Grenvillian activity in the Bamble area. Norway. Terra Abstracts 3, 504.
Lasalle, S., Dunning, G., Indares, A., 2014. In situ LA–ICP–MS dating of monazite from aluminous gneisses: insights on the tectono-metamorphic history of a granulite-facies domain in the central Grenville Province. Can. J. Earth Sci. 51, 558–572. https://doi.org/10.1139/cjes-2013-0170.
Lasalle, S., Indares, A., 2014. Anatectic record and contrasting P-T paths of aluminous gneisses from the central Grenville Province. J. Metam. Geol. 32, 627–646. https://doi.org/10.1111/jmg.12083.
Lentz, D.R., 1991. Petrogenesis of uranium-, thorium-, molybdenum-, and rare earth element-bearing pegmatites, skarns, and veins in the central metasedimentary belt of the Grenville Province, Ontario and Quebec. University of Ottawa, Canada. Unpublished PhD thesis,.
Lentz, D., 1996. U, Mo, and REE mineralization in late-tectonic granitic pegmatites, southwestern Grenville Province. Ore Geol. Rev. 11, 197–227.
Li, Z.X., Bogdanova, S.V., Collins, A.S., Davidson, A., De Waele, B., Ernst, R.E., Fitzsimons, I.C.W., Fuck, R.A., Gladkochub, D.P., Jacobs, J., Karlstrom, K.E., Lu, S., Natapov, L.M., Pease, V., Pisarevsky, S.A., Thrane, K., Vernikovsky, V., 2008. Assembly, configuration, and break-up history of Rodinia: A synthesis. Precambr. Res. 160, 179–210.
Lieftink, D.J., Nijland, T.G., Maijer, C., 1994. The behavior of rare-earth elements in high-temperature Cl-bearing aqueous fluids: results from the Ødegårdens Verk natural laboratory. Can. Mineral. 32, 149–158.
Lindroos, A., Romer, R.L., Ehlers, C., Alviola, R., 1996. Late-orogenic Svecofennian deformation in SW Finland constrained by pegmatite emplacement ages. Terra Nova 8, 567–574.
London, D., 1987. Internal differentiation of rare-element pegmatites: effects of boron, phosphorous, and fluorine. Geochim. Cosmochim. Acta 51, 403–420.
London, D., 2008. Pegmatites, Special Publication 10. The Canadian Mineralogist.
Ludwig, K.R., 1999. Isoplot/Ex Version 2.03. A geochronological toolkit for Microsoft Excel. Berkeley Geochronology Center Special Publication.
Lund, M., 2016. Columbite-tantalite and garnet geochemistry in Evje-Iveland, South Norway. University of Oslo, Norway. MSc thesis,.
Martin, R.F., De Vito, C., Pezzotta, F., 2008. Why is amazonitic K-feldspar an earmark of NYF-type granitic pegmatites? Clues from hybrid pegmatites in Madagascar. Am. Mineral. 93, 263–269. https://doi.org/10.2138/am.2008.2595.
Masson, S.L., Gordon, J.B., 1981. Radioactive mineral deposits of the Pembroke-Renfrew area. Mineral Deposits Circular 23, Ontario Geological Survey Publication.
Mattinson, J.M., 2011. Extending the Krogh legacy: development of the CATIMS method for zircon U-Pb geochronology. Can. J. Earth Sci. 48, 95–105.
Merlet, C., 1994. An accurate computer correction program for quantitative electron probe microanalysis. Microchim. Acta 114 (115), 363–376.
Möller, C., Andersson, J., 2018. Metamorphic zoning and behavior of an underthrusting continental plate. J. Metamor. Petrol. 36, 567–589.
Möller, C., Andersson, J., Dyck, B., Antal Lundin, I., 2015. Exhumation of an eclogite terrane as a hot migmatitic nappe, Sveconorwegian orogen. Lithos 226, 147–168.
Montel, J.M., Foret, S., Veschambre, M., Nicollet, C., Provost, A., 1996. Electron microprobe dating of monazite. Chem. Geol. 131, 37–53.
Müller, A., Ihlen, P.M., Snook, B., Larsen, R.B., Flem, B., Bingen, B., Williamson, B.J., 2015. The Chemistry of Quartz in Granitic Pegmatites of Southern Norway: Petrogenetic and Economic Implications. Econ. Geol. 110, 1737–1757.
Müller, A., Romer, R.L., Pedersen, R.B., 2017. The Sveconorwegian pegmatite province - thousands of pegmatites without parental granites. Can. Mineral. 55, 283–315.
Narum, B.M.M.N., Gabrielsen, R.H., Corfu, F., 2022. Tectonometamorphic history of the Østfold Gneiss Complex, Idefjorden lithotectonic unit, southeastern Norway. Nor. J. Geol. 101, 202117.
Nijland, T.G., Harlov, D.E., Andersen, T., 2014. The Bamble Sector, South Norway: a review. Geosci. Front. 5, 635–658.
Oftedahl, C., 1980. Geology of Norway. Norges Geologiske Undersøkelse, Oslo.
Oftedal, I., 1940. Enrichment of lithium in Norwegian cleavelandite-quartz pegmatites. Nor. Geol. Tidsskr. 20, 193–198.
Palin, R.M., White, R.W., Green, E.C.R., Diener, J.F.A., Powell, R., Holland, T.J.B., 2016. High-grade metamorphism and partial melting of basic and intermediate rocks. J. Metam. Geol. 34, 871–892. https://doi.org/10.1111/jmg.12212.
Passchier, C.W., Trouw, R.A.J., 1996. Microtectonics. Springer-Verlag, Heidelberg.
Paterson, S.R., Tobisch, O.T., 1992. Rates of processes in magmatic arcs - implications for the timing and nature of pluton emplacement and wall rock deformation. J. Struct. Geol. 14, 291–300.
Pedersen, S., Maaløe, S., 1990. The Iddefjord granite: geology and age. Norges Geol. Unders. Bull. 417, 55–64.
Petford, N., Gallagher, K., 2001. Partial melting of mafic (amphibolitic) lower crust by periodic influx of basaltic magma. Earth Planet. Sci. Lett. 193, 483–499.
Pouchou, J.-L., Pichoir, F., 1985. "PAP" Φ (ρZ) procedure for improved quantitative microanalysis. In: Armstrong, J.T. (Ed.), Microbeam Analysis. San Francisco Press, San Francisco, California, pp. 104–106.
Rivers, T., 2008. Assembly and preservation of lower, mid, and upper orogenic crust in the Grenville Province—Implications for the evolution of large hot long-duration orogens. Precambr. Res. 167, 237–259. https://doi.org/10.1016/j.precamres.2008.08.005.
Rivers, T., 2009. The Grenville Province as a large hot long-duration collisional orogen – insights from the spatial and thermal evolution of its orogenic fronts. Geological Society of London Special Publications 327, 405–444. https://doi.org/10.1144/SP327.17.
Rivers, T., Corrigan, D., 2000. Convergent margin on southeastern Laurentia during the Mesoproterozoic: tectonic implications. Can. J. Earth Sci. 37, 359–383. https://doi.org/10.1139/e99-067.
Rivers, T., Culshaw, N., Hynes, A., Indares, A., Jamieson, R., Martignole, J., 2012. The Grenville Orogen - A Post-LITHOPROBE Perspective, in: Tectonic Styles in Canada: The LITHOPROBE Perspective, Geological Association of Canada, Special Paper 49. J.A. Percival, F.A. Cook, and R.M. Clowes, pp. 97–236.
Rivers, T., Martignole, J., Gower, C.F., Davidson, A., 1989. New tectonic divisions of the Grenville Province, Southeast Canadian Shield. Tectonics 8, 63–84. https://doi.org/10.1029/TC008i001p00063.
Romer, R.L., Smeds, S.A., 1994. Implications of U-Pb ages of columbite-tantalites from granitic pegmatites for the Palaeoproterozoic accretion of 1.90-1.85-Ga magmatic arcs to the Baltic Shield. Precambr. Res. 67, 141–158.
Romer, R.L., Smeds, S.A., 1996. U-Pb columbite ages of pegmatites from Sveconorwegian terranes in southwestern Sweden. Precambr. Res. 76, 15–30.
Romer, R.L., Wright, J.E., 1992. U-Pb dating of columbites - a geochronological tool to date magmatism and ore-deposits. Geochim. Cosmochim. Acta 56, 2137–2142.
Rosing-Schow, N., Müller, A., Friis, H., 2018. A comparison of the mica chemistry of the pegmatite fields in southern Norway. Can. Mineral. 56, 463–488.
Schärer, U., 1984. The effect of initial Th-230 disequilibrium on young U-Pb ages - The Makalu case, Himalaya. Earth Planet. Sci. Lett. 67, 191–204.
Scherer, E., Münker, C., Mezger, K., 2001. Calibration of the lutetium-hafnium clock. Science 293, 683–687.
Schuster, R., Ilickovic, T., Mali, H., Huet, B., Schedl, A., 2017. Permian pegmatites and spodumene pegmatites in the Alps: Formation during regional scale high temperature/low pressure metamorphism, in: Müller, A., Rosing-Schow, N. (Eds.), 8th International Symposium on Granitic Pegmatites. NGF Abstracts and Proceedings, Kristiansand, Norway, pp. 122-125.
Segalstad, T.V., Raade, G., 2003. Scandium mineralizations in southern Norway – geological background for the field trip. NGF Abstracts and Proceedings 2, 57–86.
Simmons, W.B., Foord, E.E., Falster, A.U., 1996. Anatectic origin of granitic pegmatites, Western Maine, USA, GAC-MAC Annual meeting - Abstracts with Programs, University of Manitoba, Winnipeg, USA.
Simmons, W., Falster, A., Webber, K., Roda-Robles, E., Boudreaux, A.P., Grassi, L.R., Freeman, G., 2016. Bulk composition of Mt. Mica pegmatite, Maine, USA: Implications for the origin of an LCT type pegmatite by anatexis. Can. Mineral. 54, 1053–1070.
Slagstad, T., Hamilton, M.A., Jamieson, R.A., Culshaw, N.G., 2004. Timing and duration of melting in the mid orogenic crust: Constraints from U-Pb (SHRIMP) data, Muskoka and Shawanaga domains, Grenville Province, Ontario. Can. J. Earth Sci. 41, 1339–1365. https://doi.org/10.1139/e04-068.
Slagstad, T., Roberts, N.M.W., Marker, M., Røhr, T.S., Schiellerup, H., 2013. A non-collisional, accretionary Sveconorwegian orogen - Reply. Terra Nova 25, 169–171.
Slagstad, T., Roberts, N.M.W., Kukalov, E., 2017. Linking orogenesis across a supercontinent; the Grenvillian and Sveconorwegian margins on Rodinia. Gondw. Res. 44, 109–115.
Slagstad, T., Roberts, N.M.W., Coint, N., Høy, I., Sauer, S., Kirkland, C.L., Marker, M., Røhr, T.S., Henderson, I.H.C., Stormoen, M.A., Skår, Ø., Sørensen, B.E., Bybee, G.M., 2018b. Magma-driven, high-grade metamorphism in the Sveconorwegian Province, SW Norway during the terminal stages of Fennoscandian Shield evolution. Geosphere 14, 861–882.
Slagstad, T., Marker, M., Roberts, N.M.W., Saalmann, K., Kirkland, C.L., Kulakov, E., Ganerød, M., Røhr, T.S., Møkkelgjerd, S.H.H., Granseth, A., Sørensen, B.E., 2020. The Sveconorwegian orogeny – Reamalgamation of the fragmented southwestern margin of Fennoscandia. Precambr. Res. 350, 105877.
Snook, B., 2014. Towards exploration tools for high purity quartz: An example from the South Norwegian Evje-Iveland pegmatite belt, Camborne School of Mines. University of Exeter, United Kingdom.
Söderlund, U., Hellström, F.A., Kamo, S.L., 2008. Geochronology of high-pressure mafic granulite dykes in SW Sweden: tracking the P-T-t path of metamorphism using Hf isotopes in zircon and baddeleyite. J. Metam. Geol. 26, 539–560.
Stacey, J.S., Kramers, J.D., 1975. Approximation of terrestrial lead isotope evolution by a 2-stage model. Earth Planet. Sci. Lett. 26, 207–221.

Starmer, I.C., 1969. The migmatite complex of the Risør area, Aust-Agder, Norway. Nor. Geol. Tidsskr. 49, 33–56.
Starmer, I.C., 1993. The Sveconorwegian Orogeny in southern Norway, relative to deep crustal structures and events in the North Atlantic Proterozoic Supercontinent. Nor. Geol. Tidsskr. 73, 109–132.
Steffenssen, G., Müller, A., Munnik, F., Friis, H., Erambert, M., Kristoffersen, M., Rosing-Schow, N., 2020. Unusual scandium enrichments of the Tørdal pegmatites, south Norway. Part I: Garnet as Sc exploration pathfinder. Ore Geol. Rev. 126, 103729 https://doi.org/10.1016/j.oregeorev.2020.103729.
Stephens, M.B., Wahlgren, C.H., 2020. Chapter 15 – Polyphase (1.9-1.8, 1.5-1.4 and 1.0-0.9 Ga) deformation and metamorphism of Proterozoic (1.9-1.2 Ga) continental crust, Eastern Segment, Sveconorwegian orogen. Geological Society London Memoirs 50, 351-396.
Stuck, T.J., Diener, J.F.A., 2018. Mineral equilibria constraints on open-system melting in metamafic compositions. J. Metam. Geol. 36, 255–281. https://doi.org/10.1111/jmg.12292.
Timmermann, H., Jamieson, R.A., Parrish, R.R., Culshaw, N.G., 2002. Coeval migmatites and granulites, Muskoka domain, southwestern Grenville Province, Ontario. Can. J. Earth Sci. 39, 239–258.
Torgersen, E., Arntsen, M.L., Bingen, B., Gasser, D., Gunleiksrud, I.H., Nilsson, C., et al., 2021. Bedrock map of Norway, 1:1350000. Norges Geologiske Undersøkelse, Trondheim, Norway.
Touret, J.L.R., Hartel, T.H.D., 1990. Synmetamorphic fluid inclusions in granulites, in: Vielzeuf, D., Vidal, Ph. (Eds.), Granulites and Crustal Evolution, NATO ASI Series C, vol. 311. Kluwer, Dordrecht, pp. 397-417.
Tucker, R.D., Gower, C.F., 1994. A U-Pb geochronological framework for the Pinware Terrane, Grenville Province, Southeast Labrador. J. Geol. 102, 67.
Turlin, F., André-Mayer, A.-S., Moukhsil, A., Vanderhaeghe, O., Gervais, F., Solgadi, F., Groulier, P.-A., Poujol, M., 2017. Unusual LREE-rich, peraluminous, monazite- or allanite-bearing pegmatitic granite in the central Grenville Province, Québec. Ore Geol. Rev. 89, 627–667. https://doi.org/10.1016/j.oregeorev.2017.04.019.
Turlin, F., Deruy, C., Eglinger, A., Vanderhaeghe, O., André-Mayer, A.-S., Poujol, M., Moukhsil, A., Solgadi, F., 2018. A 70 Ma record of suprasolidus conditions in the large, hot, long-duration Grenville Orogen. Terra Nova 30–3, 233–243. https://doi.org/10.1111/ter.12330.
Turlin, F., Vanderhaeghe, O., Gervais, F., André-Mayer, A.-S., Moukhsil, A., Zeh, A., Solgadi, F., I.P.T.N., 2019. Petrogenesis of LREE-rich pegmatitic granite dykes in the central Grenville Province by partial melting of Paleoproterozoic-Archean metasedimentary rocks: Evidence from zircon U-Pb-Hf-O isotope and trace element analyses. Precambrian Research 327, 327-360.
Tuttle, O.F., Bowen, N.L., 1958. Origin of granite in the light of experimental studies in the system $NaAlSi_3O_8$–$KAlSi_3O_8$–$SiO_2$–$H_2O$. Geological Society American Memoirs 74, 1–145.
Van Gool, J.A.M., Rivers, T., Calon, T., 2008. Grenville Front zone, Gagnon terrane, southwestern Labrador: Configuration of a midcrustal foreland fold-thrust belt. Tectonics 27, TC1004. https://doi.org/10.1029/2006TC002095.
Vander Auwera, J., Bogaerts, M., Liégeois, J.-P., Demaiffe, D., Wilmart, E., Bolle, O., Duchesne, J.C., 2003. Derivation of the 1.0-0.9 Ga ferro-potassic A-type granitoids of southern Norway by extreme differentiation from basic magmas. Precambr. Res. 124, 107–148.
Vander Auwera, J., Bolle, O., Bingen, B., Liégeois, J.-P., Bogaerts, M., Duchesne, J.C., De Waele, B., Longhi, J., 2011. Sveconorwegian massif-type anorthosites and related granitoids result from post-collisional melting of a continental arc root. Earth Sci. Rev. 107, 375–397.
Vander Auwera, J., Bolle, O., Dupont, A., Pin, C., Paquette, J.-L., Charlier, B., Duchesne, J.C., Mattielli, N., Bogaerts, M., 2014. Source-derived heterogeneities in the composite (charnockite-granite) ferroan Farsund intrusion (SW Norway). Precambr. Res. 251, 141–163. https://doi.org/10.1016/j.precamres.2014.06.003.
Venugopal, D.V., 1970. Geology and structure of the area west of Fyresvatn, Telemark. Universitetsforlaget, Oslo, Norway, Southern Norway.
Viola, G., Henderson, I.H.C., Bingen, B., Henriks, B.W.H., 2011. The Grenvillian-Sveconorwegian orogeny in Fennoscandia: Back-thrusting and extensional shearing along the «Mylonite Zone». Precambr. Res. 189, 368–388.
Webber, K., Simmons, W.B., Falster, A.U., Hanson, S.L., 2019. Anatectic pegmatites of the Oxford County pegmatite field, Maine, USA. In: Wise, M., Brown, C., Simmons, W.B., Roda-Robles, E., Webber, K. (Eds.), 9th International Symposium on Granitic Pegmatites. Pala, California, USA, pp. 87–90.
Wolf, M.B., Wyllie, P.J., 1994. Dehydration-melting of amphibolite at 10 kbar: The effects of temperature and time. Contrib. Miner. Petrol. 115, 369–383. https://doi.org/10.1007/BF00320972.
Wyllie, P.J., Wolf, M.B., 1993. Amphibolite dehydration-melting: Sorting out the solidus. Geol. Soc. Lond. Spec. Publ. 76, 405–416. https://doi.org/10.1144/GSL.